

1 **Evaluating modelling decisions and spatial predictions in ecosystem**

2 **mapping**

3 **Authors:**

4 Alys R. Young<sup>1,2,3</sup>, Nicholas J. Murray<sup>3</sup>, Jane Elith<sup>2</sup>, Brett A. Bryan<sup>1</sup>, Hugh F. Davies<sup>4,5</sup>, and Emily

5 Nicholson<sup>2</sup>

6 **Affiliations:**

7 <sup>1</sup> School of Life and Environmental Sciences, Faculty of Science, Engineering, and Built

8 Environment, Deakin University, Burwood VIC 3125 Australia

9

10 <sup>2</sup> School of Agriculture, Food and Ecosystem Science, Faculty of Science, The University of

11 Melbourne, Parkville VIC 3010 Australia

12

13 <sup>3</sup> College of Science and Engineering, James Cook University, Townsville QLD 4811 Australia

14

15 <sup>4</sup> Research Institute for the Environment and Livelihoods, Charles Darwin University, Casuarina

16 NT 0909 Australia

17

18 <sup>5</sup> School of Environmental and Rural Science, Faculty of Agriculture, Business and Law,

19 University of New England, Armidale, NSW 2350 Australia

20 **Corresponding author:**

21 Alys R. Young

22 [alys.young@jcu.edu.au](mailto:alys.young@jcu.edu.au)

23 [aalsy.research@gmail.com](mailto:aalsy.research@gmail.com)

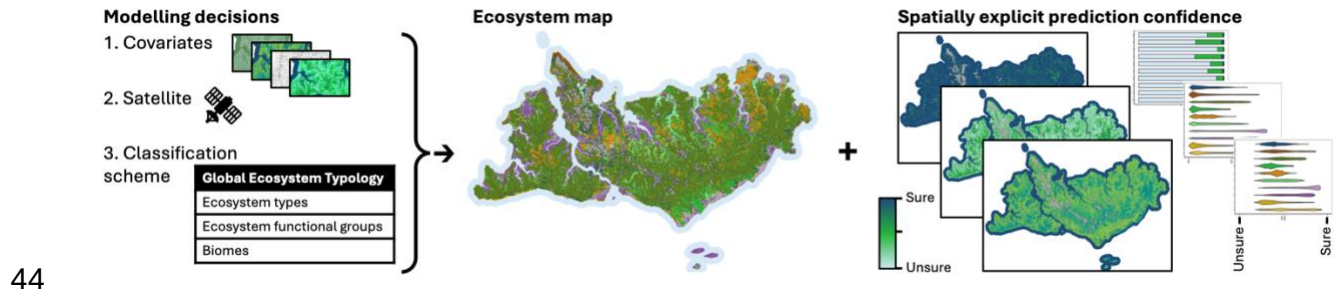
24 ORCID 0000-0002-9562-2253

25

26 **Abstract**

27 Ecosystem maps support a vast array of applications in conservation, land management, and  
28 policy. The capacity of such an ecosystem map to support these applications is determined by  
29 its accuracy and in turn by the decisions made the modelling procedure. We evaluated the  
30 influence of select modelling decisions for a pixel-based, random forest classification model  
31 used to map ecosystems for the remote Tiwi Islands, Australia. Across the three modelling  
32 decisions of classification scheme using the Global Ecosystem Typology, satellite sensor  
33 selection between Landsat-9 and Sentinel-2, and covariate set composition by including  
34 additional data sources, we evaluated model performance using multiple metrics and produced  
35 spatially explicit uncertainty maps to communicate map limitations. Covariates additional to  
36 those from satellite images consistently improved model performance, representing the most  
37 impactful pathway to accuracy gains without sacrificing ecological detail unlike class  
38 aggregation. The choice of satellite and sensor provided smaller accuracy gains, with Landsat-9  
39 acquisitions generally outperforming Sentinel-2, potentially because the spatial heterogeneity  
40 of ecosystems is modulated by the coarser resolution. Uncertainty maps are practical and  
41 accessible tools for producers to communicate limitations which is critical information for  
42 decision-making and achieving conservation goals.

43 **Graphical abstract**



45 **Key words:**

46 Remote sensing, Earth observation, vegetation mapping, land cover, island ecology, tropical

47 savanna, machine learning, biogeography



49 Ecosystem distribution maps form a crucial foundation to understand, monitor, and make  
50 decisions about the environment. Applications of ecosystem maps span conservation  
51 assessments (Murray *et al.*, 2017; Keith, Ferrer-Paris, *et al.*, 2024), spatial planning (Watson *et*  
52 *al.*, 2023; Keith, Ghoraba, *et al.*, 2024), valuing services (Hein *et al.*, 2020; Xiao *et al.*, 2024) and  
53 reporting (Watson *et al.*, 2020; Nicholson *et al.*, 2024). The usefulness of an ecosystem map in  
54 these contexts is determined by its ability to accurately model and represent the distributions  
55 of ecosystem classes in geographic space.

56  
57 As ecosystem maps are models of the natural world, decisions made during the modelling  
58 process can strongly impact outcomes (Gould *et al.*, 2023). Variations due to modelling  
59 decisions, model uncertainty, and errors (henceforth, 'map reliability') impedes comparisons of  
60 map results between years and regions, hindering our ability to track changes over time or  
61 make landscape scale assessments. Further, map reliability propagates through to applications  
62 (Burgman, Lindenmayer and Elith, 2005; Jansen *et al.*, 2022), influencing area estimates  
63 (Olofsson *et al.*, 2020; Naas *et al.*, 2023), ecosystem accounting (Venter *et al.*, 2024), and  
64 assessments (De la Cruz *et al.*, 2017). Such inaccuracies and variations hamper the conservation  
65 of ecosystems. As the need for ecosystem maps grow to support national reporting on the  
66 Global Biodiversity Framework, so too does the importance of understanding the impact of  
67 modelling decisions specifically for ecosystems.

68

69

70 Key factors of model formulation known to influence maps relate to 1) the typology being  
71 mapped, 2) errors in the training data, 3) choice of model covariates, and 4) model types.  
72 Locally relevant typologies achieve higher accuracies than re-using typologies from other  
73 locations (Fagua *et al.*, 2023), while typologies that miss classes produce biased accuracy  
74 assessments (Foody, 2021). Aggregating classes is a common approach touted to improve  
75 accuracy despite with limited evidence (Yu *et al.*, 2014). Accurate classification models rely on  
76 accurate training data (Rocchini *et al.*, 2013), although machine learning models can handle  
77 some level of error (Foody *et al.*, 2016; Gong *et al.*, 2019; Venter and Sydenham, 2021).  
78 Decisions around the covariates to use are prominent in ecosystem mapping (Simensen *et al.*,  
79 2020; Liu *et al.*, 2023; Trouvé *et al.*, 2023; Naas *et al.*, 2024) and for land use/land cover classes  
80 (Yu *et al.*, 2014; Khatami, Mountrakis and Stehman, 2016; Zeferion *et al.*, 2020; Ghayour *et al.*,  
81 2021; Venter and Sydenham, 2021), with studies consistently showing an improvement to  
82 model accuracies with covariates additional to optical satellite data. The type of model used is  
83 also extensively tested, although there is no clear winner across studies (Yu *et al.*, 2014;  
84 Khatami, Mountrakis and Stehman, 2016; Talukdar *et al.*, 2020; Ghayour *et al.*, 2021; Prasad *et*  
85 *al.*, 2022), spurred on by the proliferation of machine learning models.

86

87 Evaluating modelling decisions is common in other spatial modelling applications. These fields  
88 include landcover mapping which typically focus on structural elements of the landscape, land-  
89 use mapping, and species distribution models (Khatami, Mountrakis and Stehman, 2016;  
90 Grimmett, Whitsed and Horta, 2020). Fewer studies have examined the impacts of model  
91 formulation in ecosystem mapping which presents a unique and challenging case study  
92 (Rocchini *et al.*, 2013).

93

94 Ecosystems are defined by a unique biotic community, the abiotic environment, and driving  
95 ecological processes (CBD, 1992). Thus, ecosystem classes can be difficult to visibly distinguish  
96 using remotely sensed data. For instance, forest ecosystem types delineated by distinct  
97 understories but displaying similar canopy composition and physical structure are  
98 indistinguishable with multispectral imagery (Trouvé *et al.*, 2023). Ecosystems also have  
99 complex spatiotemporal dynamics because of ecological processes, natural variation, and  
100 disturbance (Dryflor *et al.*, 2016; Dorrough *et al.*, 2021; Keith *et al.*, 2022). Finally, the number  
101 of ecosystem types are typically higher than in landcover classification, presenting a crucial  
102 challenge for accurate mapping (Yu *et al.*, 2014). For instance, the 73 landcover classes in the  
103 South African national map are referable to 456 terrestrial ecosystems (Skowno and Monyeki,  
104 2021), while 98 ecosystem types are described for Italy compared to 66 landcover classes  
105 (Capotorti *et al.*, 2023) and 81 ecosystems compared to 54 land cover types in Colombia (Etter  
106 *et al.*, 2020).

107

108 In addition to understanding the impact of modelling decisions, there is a long and growing  
109 interest in communicating remaining uncertainty in the output map. Spatially explicit  
110 evaluation metrics (henceforth, ‘uncertainty maps’) have emerged to communicate map  
111 reliability in response to limitations of current evaluation assessments (Stehman and Foody,  
112 2019; Foody, 2021) and as a result of modelling advances (Loosvelt *et al.*, 2012; Mitchell,  
113 Downie and Diesing, 2018). Traditional approaches to map evaluation compare the known class  
114 and the model predicted class for an independent dataset through a confusion matrix (Foody,  
115 2002) to calculate evaluation metrics, such as the proportion of correctly predicted classes (i.e.,  
116 accuracy). However, confusion matrices and subsequent evaluation metrics are strongly  
117 impacted by the sampling scheme used to collect the data, the sample size of each class, and  
118 errors in the original datasets (Foody, 2002). Uncertainty maps complement confusion matrices  
119 by emphasising spatial patterns and facilitate uncertainty propagation into downstream  
120 analyses (Foody, 2002; Jansen *et al.*, 2022). Here, we use the term ‘uncertainty map’ to  
121 facilitate interpretation, acknowledging that these metrics are calculated from the proportion  
122 of trees voting for a class membership instead of a true probability (McIver and Friedl, 2001;  
123 Mitchell, Downie and Diesing, 2018) and that high confidence is not synonymous with high  
124 accuracy (Stehman and Foody, 2019). Despite the prominence of conveying and handling  
125 uncertainty in ecology (Jansen *et al.*, 2022), uncertainty maps are yet to become standard  
126 practice and require further demonstrations in new applications.

127

128 In this paper, we sought to evaluate the effects of modelling decisions on ecosystem maps,  
129 using the case study of the Tiwi Islands, Australia. On the Indigenous-owned and managed  
130 islands, ecosystem maps inform development decisions and management actions (e.g. Richards  
131 *et al.*, 2012). We tested the sensitivity of the map reliability to three modelling decisions. Firstly,  
132 to represent decisions related to the classification scheme, we used a recently developed  
133 hierarchical ecosystem typology (Young *et al.*, 2025) that is aligned with the Global Ecosystem  
134 Typology (GET), the internationally accepted classification of ecosystems (UNSD, 2021; Keith *et*  
135 *al.*, 2022). Different levels of a classification hierarchy are ideal for systematically testing the  
136 number of classes which change in relation to the thematic resolution (also called ‘thematic  
137 scale’ or ‘class resolution’). Secondly, to examine the impact of the choice of satellite, we  
138 compared model covariates retrieved from the Landsat-9 satellite with the Operational Land  
139 Imager (OLI-2) sensor against the Sentinel-2 satellite with the Multispectral imager  
140 (MSI) sensor. The Landsat and Sentinel missions represent two flagship programs providing  
141 open-access satellite images (Wulder *et al.*, 2012) and vary in spatial and spectral resolution,  
142 length of time series and processing. Thirdly, to assess the implications of model covariates on  
143 map reliability, we investigated the use of only satellite image covariates and compared these  
144 to models that also include other ecologically meaningful covariates (hereafter, “additional”  
145 covariates). To further communicate model uncertainty, we demonstrate three uncertainty  
146 maps to accompany the ecosystem map which can inform managers of map reliability and  
147 improve conservation outcomes.

## 148 **2. Materials and methods**

149 **2.1 Case study location**

150 The Tiwi Islands, including Melville Island (5,788 km<sup>2</sup>), Bathurst Island (1,693 km<sup>2</sup>) and  
151 numerous small islands, are located off the northern coast of the Northern Territory, Australia.  
152 The Tiwi Islands are in the Australian “Tiwi-Coburg” bioregion (DCCEEW, 2021) and the global  
153 “Arnhem Land tropical savanna” ecoregion (Olson *et al.*, 2001). The lands and waters of the  
154 Tiwi Islands are managed by the Indigenous Tiwi peoples. Much of the Islands are remote and  
155 challenging to access (**Error! Reference source not found.**).

156 **2.2 Classification scheme**

157 To investigate the impact of the number of classes in the classification scheme which change in  
158 relation to the thematic resolution, we employed a recent typology of Tiwi Island ecosystem  
159 types (Young *et al.*, 2025) developed using the GET and with a known relationship to each GET  
160 level. We tested classification schemes for mapping at three levels of the GET hierarchy: the  
161 finest thematic resolution level 6 ‘subglobal ecosystem types’ with 11 classes, level 3  
162 ‘ecosystem functional groups’ (EFGs) with 10 classes, and level 2 ‘biome’ as the coarsest  
163 resolution with eight classes (Table 1). Here we use the term ‘biome’ as defined by the GET;  
164 biomes represent the subdivision of realms (e.g. fresh water) by similar broad features of  
165 ecosystem structure and function (Keith *et al.*, 2022), although recognise other popular  
166 definitions (Mucina, 2019).

167 Table 1. Details of how the ecosystem types were grouped into the ecosystem functional group  
168 and biome classification schemes according to the Global Ecosystem Typology, and the data  
169 sources employed for each class to develop the reference points.

Classification schemes				Data sources for each ecosystem								
Biome (Level 2)	Ecosystem Functional Group (Level 3)	Tiwi Island mapped ecosystem types (Level 6)	Tiwi Island ecosystem typology (Level 6)	Wildlife aerial survey photos	Visits with Tiwi knowledge authorities	Tiwi Plantation Corporation maps	Threatened species monitoring	Tiwi Plantation Corporation surveys	Consultancy reports	Vegetation mapping aerial photos	Targeted vegetation mapping	Shoreline erosion maps
	T1.1			X	X	X	X	X				
T1 Tropical-subtropical forests biome (n = 1575)	Tropical/Subtropical lowland rainforests (n = 433)	Wet rainforest (n = 433)	Wet rainforest									
	T1.2			X	X	X			X			
	Tropical/Subtropical dry forests and thickets (n = 1142)	Dry rainforest (n = 1142)	Dry rainforest									
T3 Shrublands and shrubby woodlands (n = 214)	T3.1 Seasonally dry tropical shrublands (n = 214)	Treeless plains (n = 214)	Treeless plains	X	X				X	X	X	
			Eucalypt open forest	X	X		X			X		
T4 Savannas and grasslands (n = 1023)	T4.2 Pyric tussock savannas (n = 1023)	Eucalypt savanna (n = 927)	savanna									
			Eucalypt and mixed-species savanna									
		Melaleuca savanna (n = 96)	Melaleuca savanna	X						X	X	
TF1 Palustrine wetlands biome (n = 704)	TF1.4 Seasonal floodplain marshes (n = 704)	Grasslands and sedgelands (n = 704)	Grasslands and sedgelands	X								
MFT1 Brackish tidal (n = 998)	MFT1.2 Intertidal forests and shrublands (n = 698)	Mangroves (n = 698)	Mangroves	X	X					X		

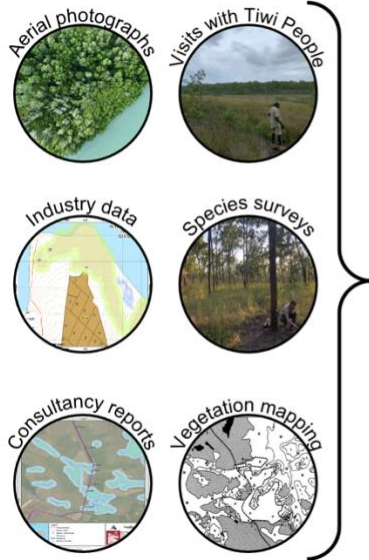
	MFT1.3 Coastal			X	X		
	saltmarshes and reedbeds (n = 300)	Coastal saltmarsh (n = 300)	Coastal saltmarsh				
MT1 Shorelines biome (n = 428)	MT1.3 Sandy shorelines (n = 428)	Shorelines (n = 428)	Sandy beaches	X	X	X	X
			Rocky shorelines		X		
MT2 Supralittoral coastal biome (n = 531)	MT2.1 Coastal shrublands and grasslands (n = 531)	Sand dunes (n = 531)	Sand dunes	X		X	X
Water (n = 414)	Water (n = 414)	Water (n = 414)	Ocean	X	X		X
			Freshwater				

170

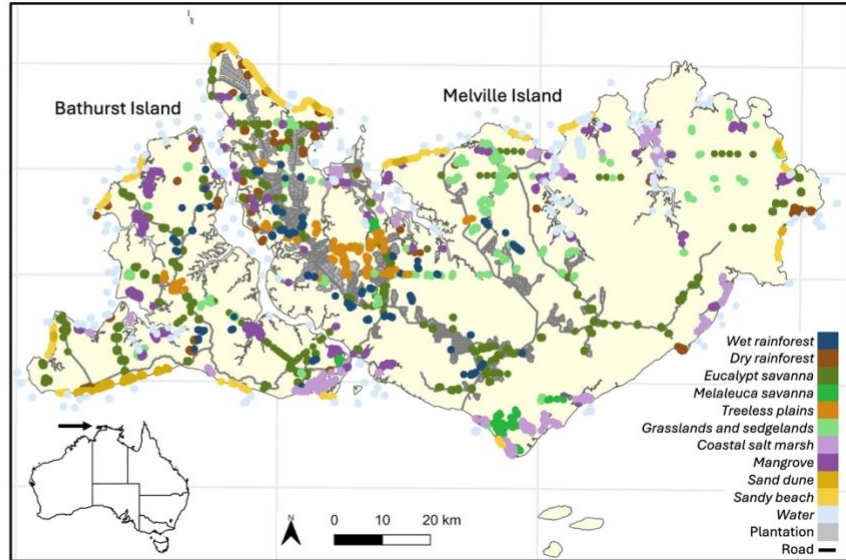
### 171 2.3 Reference points

172 Reference points (or ‘training points’) are confirmed occurrences of each ecosystem class in the  
 173 classification scheme. We employed the reference point collection developed in Young et al.,  
 174 2025 but describe the methods in more detail here. For an overview of the full methodology,  
 175 see Appendix S1 in the Supporting Information.

1) Collate data sources



2) The resulting reference points



176

177 Figure 1. The types of data sources collated from a database managed by the Tiwi Land Council  
178 and used to place reference points, and the final reference point locations used to model the  
179 distribution of 11 ecosystems (colours) for the Tiwi Islands, Australia.

### 180 **2.3.1 Data collation**

181 We developed reference points by first collating diverse spatial datasets with information  
182 related to ecosystems available in a database owned by the Tiwi Land Council, and field visits  
183 with Tiwi knowledge authorities (Table 1). We used these datasets to identify areas with  
184 ecosystems and then place labelled points, described next in section 2.3.2. The spatial datasets  
185 available were collected by numerous academic and industry professionals over 35 years, and  
186 included various types of data, such as aerial photographs, high-quality industry maps, and  
187 ecological surveys (Figure 1). For the aerial photographs taken from helicopters for animal and  
188 vegetation surveys, we labelled each photograph with the ecosystems that were visible and  
189 retained only highly confident labels. We used GPS tracks, PDF maps, and field notes from Tiwi  
190 Plantation Corporation to locate rainforest patches. Consultancy reports and development  
191 proposals contained vegetation maps and photographs, and information regarding ecosystem  
192 processes (EcOz Environmental Services, 2012; EcOz Environmental Consultants, 2021).  
193 Rainforest patches were further located using fauna, flora, and threatened species surveys  
194 (Russell-Smith, 1991; Menkhorst and Woinarski, 1992; Gambold and Woinarski, 1993; Liddle  
195 and Elliott, 2008). *Eucalypt savannas* have been surveyed for mammals and threatened fauna  
196 (Davies *et al.*, 2018, 2019; Davies, Rangers, Rees, *et al.*, 2021; Neave *et al.*, 2024). Vegetation  
197 communities of the *treeless plains* ecosystem (Wilson and Fensham, 1994) and *Melaleuca*  
198 *savanna* (Brocklehurst and Lynch, 2001, 2009) have been the focus of previous mapping efforts.  
199 From 2021 to 2023, we undertook on-ground visits with Tiwi knowledge authorities to locations  
200 and ecosystem types chosen by the Tiwi knowledge authorities.

### 201 **2.3.2 Reference point placement**

202 For each ecosystems type, we consulted and visualised all collated datasets simultaneously with  
203 recent satellite imagery and the Sentinel-2 and Landsat-9 imagery (described in Section 2.4) to  
204 place initial reference points on a 30 m x 30 m grid at or near to the locations identified in the  
205 collated datasets through visual interpretation in QGIS (QGIS Development Team, 2018). All  
206 points located in uncertain ecosystem classes were removed. We checked each point with the  
207 satellite imagery used in the modelled to ensure the ecosystems had not changed between  
208 when the collated datasets were collected. The datasets produced and owned by Tiwi  
209 Plantation Corporation facilitated the identification reference points due to their high spatial  
210 accuracy. Developing reference points for the *treeless plains* maps was challenged by the low  
211 spatial detail in the line drawn maps and land use change since this time. Aerial photographs  
212 provided essential information in remote areas. From the initial reference points, we removed  
213 all points closer than 100 m to minimise spatial autocorrelation and inflated evaluation metrics  
214 (Stehman, 2009; Stehman and Foody, 2019) using the 'enmSdmX' package with R in R-studio (R  
215 Core Team, 2018; RStudio Team, 2020; Smith *et al.*, 2023). This process yielded 5,887 reference  
216 points for the remainder of the analysis (Table 1, Figure 1). We obtained too few reference  
217 points to map *rocky shorelines* as this ecosystem was only identified from visits with Tiwi  
218 knowledge authorities. None of the collated datasets distinguished marine and freshwater  
219 ecosystems, and hence have been modelled together as *water* in this research. For all software  
220 details, see the Appendix 2.2.

## 221 **2.4 Satellite image processing**

222 To test the choice of satellite and sensor, we retrieved images acquired by the OLI-2 sensor  
223 onboard the Landsat-9 satellite (level 2, collection 2, tier 1), courtesy of the United States  
224 Geological Survey, and the MSI sensor on the Sentinel-2 satellite from the surface reflectance  
225 harmonised collection (level-2A) with atmospheric correction, courtesy of the European Space  
226 Agency. In this paper, we refer to these two data sources as ‘Landsat-9’ and ‘Sentinel-2’ for  
227 succinctness, recognising that each satellite also represents different sensors, wavelengths  
228 measured, return times, and other attributes. We obtained and processed the images using  
229 Google Earth Engine via the ‘rgee’ and ‘rgeeExtra’ packages in R (Gorelick *et al.*, 2017; Aybar *et*  
230 *al.*, 2020).

231

232 Clouds and smoke are common above the Tiwi islands. We tested multiple approaches for  
233 developing cloud-free images suitable for modelling. We compiled image sets based on the  
234 starting date (January, February, or March) and ending date (April or May) to capture images  
235 prior to prescribed burning, from one-year (2023), two-year (2022 and 2023), or three-year  
236 (2021 to 2023) periods. During these years, there were no known changes in the extent of  
237 natural ecosystems and targeted investigations supplementary to this research showed only  
238 localised changes in mangroves which is not discussed further. We filtered the image sets by  
239 four cloud cover limits (20%, 30%, 40% and 50%), masked the remaining clouds (see Appendix  
240 S3 for methods) and then reduced the image sets to a single image by the median value of each  
241 pixel. We inspected the resultant 120 images for residual clouds. We selected the method that  
242 minimised 1) the residual cloud to reduce errors that would affect the models, 2) the number of  
243 years to limit the impact of landscape change, and 3) the cloud cover limit to include the most  
244 images.

245

246 The final Landsat-9 composite image was developed from images acquired over January to May  
247 in 2023 with less than 30% cloud cover. The final Sentinel-2 image was a three-year composite  
248 (2021 to 2023) of images acquired from January to May each year with less than 20% cloud  
249 cover.

## 250 **2.5 Environmental covariates**

251 To develop covariates for testing, we extracted four bands for the red, green, blue, and near-  
252 infrared wavelengths from the two satellite images and calculated the normalised difference  
253 vegetation index (NDVI). For the additional covariates, we obtained soil composition layers  
254 from the Soil and Landscape Grid of Australia (Viscarra Rossel *et al.*, 2015) and calculated a  
255 mean for each layer in the top 30 cm and 2 m of soil. We obtained elevation data from the  
256 Shuttle Radar Topography Mission (SRTM) 5-m Smoothed Digital Elevation Model (DEM-S)  
257 (Gallant *et al.*, 2009) and created the Topographic Roughness Index and slope (in degrees) using  
258 the ‘terra’ package (Hijmans, 2023). We also investigated the height above which 50%, 75% and  
259 95% of the vegetation biomass exists (Scarth *et al.*, 2023). Data sources and detailed  
260 descriptions are available in Appendix S4.

261

262 To predict the ecosystem distribution across an area with the model, the covariate rasters for  
263 each predictor must be available spatially, in the same resolution, and same projection. We  
264 resampled the covariates using bilinear interpolation to the resolution of the visible bands of  
265 each satellite (~30 m for OLI-2 sensor on the Landsat-9 satellite and ~10 m for MSI sensor on  
266 the Sentinel-2 satellite) and the GDA2020 MGA52S coordinate reference system (EPSG: 7852).

267

268 Correlations among predictor covariates are known to bias inference and affect parameter  
269 estimates (Dormann *et al.*, 2013). We tested collinearity using Pearson’s correlation coefficient,  
270 retaining covariates with pairwise correlations of less than 0.7 (Appendix S4). For the satellite  
271 image covariate set, we retained red, near-infrared, and NDVI. For the satellite image and  
272 additional covariate set, we retained red, near-infrared, NDVI, elevation, slope, height of 50% of  
273 the vegetation biomass, and the organic carbon, silt and clay in the top 30 cm of soil.

## 274 **2.6 Model formulation and fitting**

275 We tested 12 model formulations consisting of combinations of three modelling decisions. For  
276 the three classification schemes, two satellites, and two covariate sets (total of 12  
277 formulations), we fitted supervised, pixel-based random forest classification models weighting  
278 each class by the number of reference points using the ‘ranger’ package (Wright and Ziegler,  
279 2017). We parameterised the models to optimise performance while minimising overfitting  
280 using a grid search. We built models with all combinations of the number of trees from 10 to  
281 200 in intervals of 10, the number of covariates options to split the nodes from one to five, and  
282 a tree depth of the even numbers from two to 10 as well as one. The optimal parameters were  
283 110 trees, two splitting covariates, and six nodes deep. We employed these parameter settings  
284 across all models for consistency. After parameterisation, we fitted models for the 12  
285 formulations using a cross-validation procedure. We randomly assigned the reference points to  
286 one of five partitions, built the cross-validated models on four of the five partitions and tested  
287 on the held-out partition, producing a total of 60 models.

## 288 **2.7 Model evaluation**

289 From the cross-validated models, we extracted the variable importance by the permutation and  
290 summed the predicted classes for the held-out partition to produce a confusion matrix. From  
291 the confusion matrices, we calculated the overall evaluation metrics of the accuracy and kappa,  
292 and obtained the out-of-bag error from the model output.

293

294 Although the use of kappa remains the subject of debate (Pontius Jr and Millones, 2011; Foody,  
295 2020), we report on it here to facilitate comparisons with other studies as it is still widely used  
296 (Morales-Barquero *et al.*, 2019). We used the by-class evaluation metrics of sensitivity,  
297 specificity, precision, F1, and negative predicted value. All evaluation metrics were calculated  
298 using the 'caret' package (Kuhn, 2008) using the equations in the Appendix 2.5. We tested the  
299 sensitivity of the overall model evaluation metrics to the cross-validation procedure by running  
300 10,000 models for each formulation on a random 80% of the data and predicting to the  
301 remaining 20%.

## 302 **2.8 Model prediction**

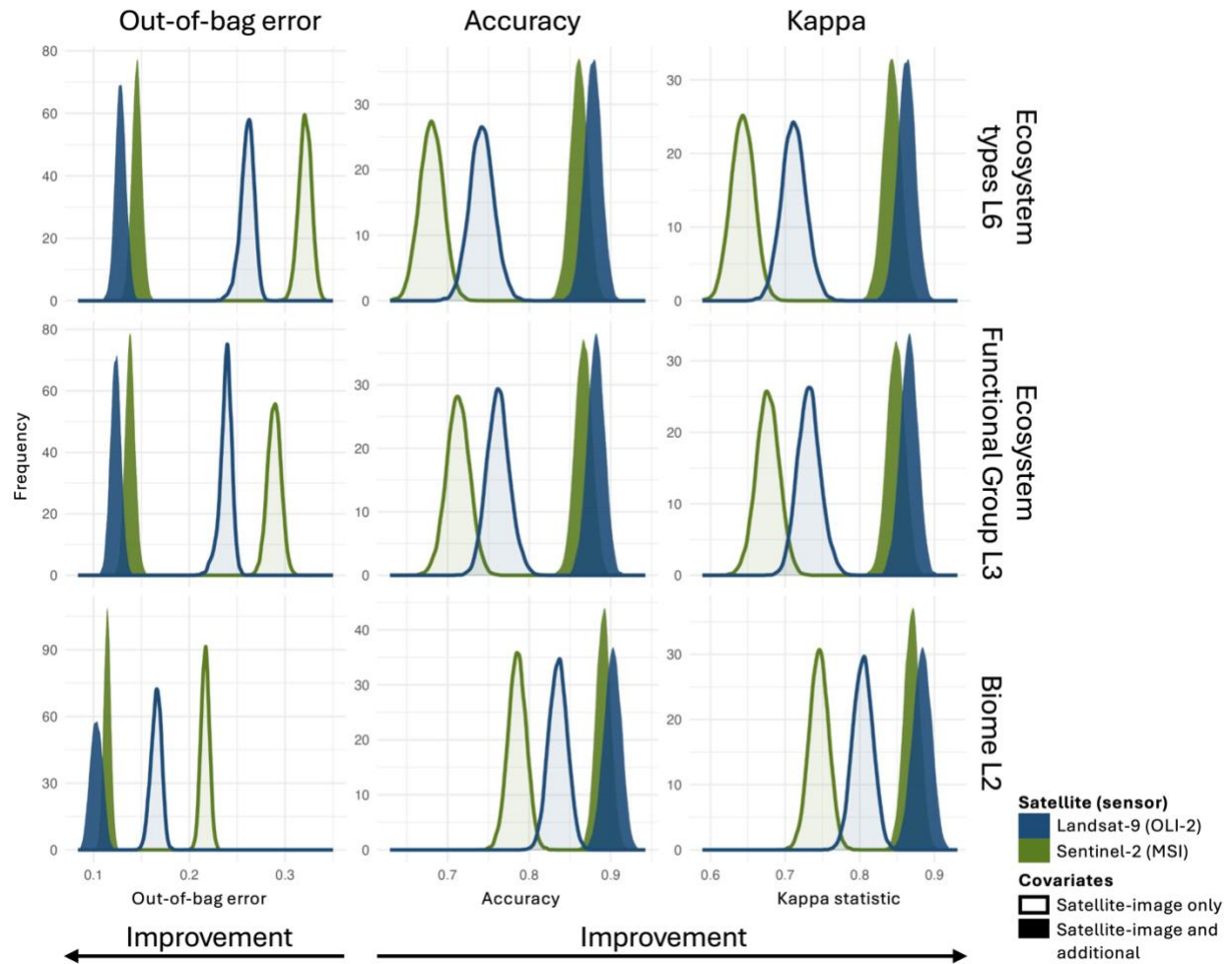
303 To map the spatial distribution of ecosystems, we predicted each class for every pixel using the  
304 cross-validated models. The proportion of trees in the random forest trees that assigned the  
305 pixel to a class is commonly referred to as a pseudo-probability. The class with the highest  
306 pseudo-probability is the final predicted class for that pixel. We identified the predicted class  
307 for each model formulation as the mode of the most probable class from the cross-validated  
308 models. In the extremely rare case when multiple classes were predicted in equal amounts, we  
309 selected the class with the highest mean pseudo-probability. We then visualised the predicted  
310 class to map ecosystem distribution and overlaid maps of the modified areas.

## 311 **2.9 Uncertainty maps**

312 To communicate the reliability of the spatial distributions, we produced three uncertainty  
313 maps. Across the cross-validated models for each pixel, we calculated the mean pseudo-  
314 probability of the highest class (henceforth, maximum probability; McIver and Friedl, 2001;  
315 Loosvelt *et al.*, 2012), the mean difference between the highest and second highest pseudo-  
316 probabilities (henceforth, 'Margin of Victory', MoV; McIver and Friedl, 2001) and the number of  
317 unique predicted classes (henceforth, prediction stability; Grimmett, Whitsed and Horta,  
318 2020). Both the maximum probability and the MoV express the strength of the class assignment  
319 compared to the other class options. The prediction stability indicates the repeatability within  
320 replicates of the same algorithm.

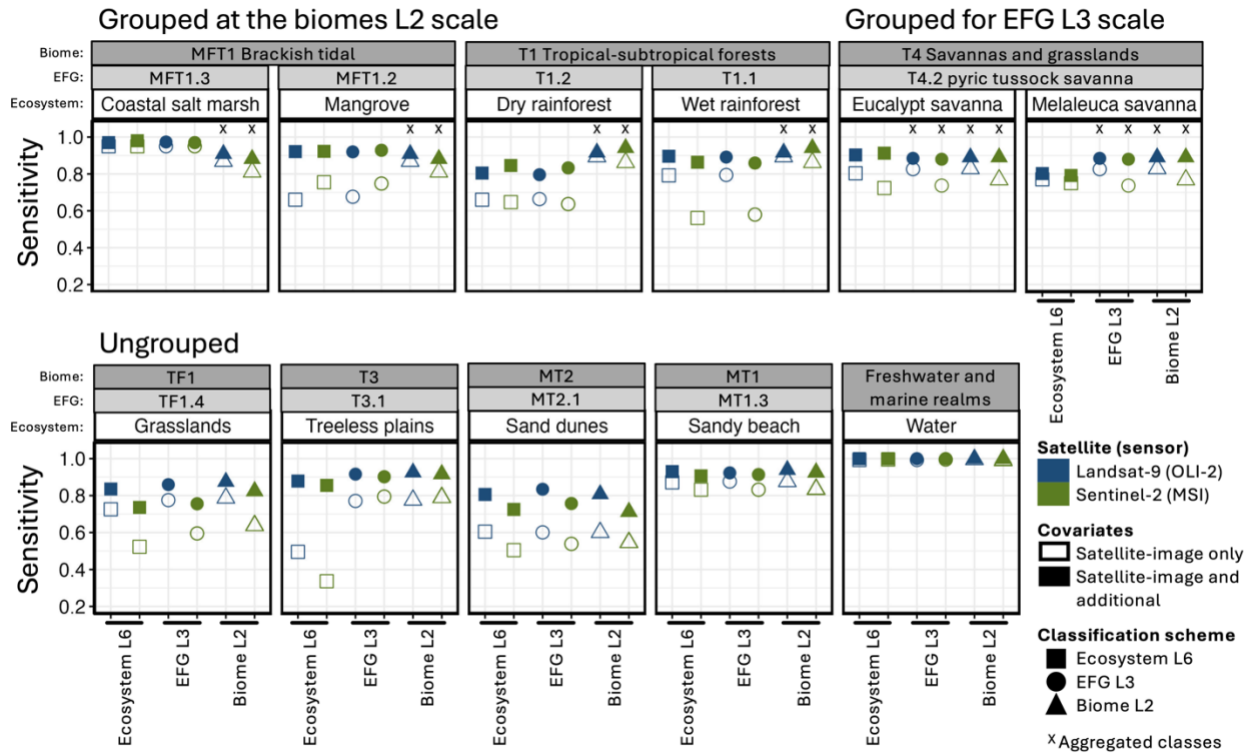
## 321 **3. Results**

322 We found that choice of covariates most strongly impacted model output. First, using the  
323 satellite image and additional covariates together improved the overall evaluation metrics  
324 across all model formulations (Figure 2 and Appendix S6). Most classes also improved in by-  
325 class metrics (Figure 3) with few exceptions. The most pronounced improvements were in the  
326 *treeless plains*, *Melaleuca savanna*, and the *wet and dry rainforest* ecosystems (Figure 3 and  
327 Appendix S6). Not all additional covariates contributed equally. On these relatively flat islands,  
328 elevation proved the most important additional covariate, while the soil covariates and slope  
329 added little explanatory power (Appendix S6).



330

331 Figure 2. The distribution of the overall evaluation metrics using out-of-bag error (left column),  
 332 accuracy (centre column) and kappa statistic (right column) from 10,000 random forest models  
 333 built on a random 80% of the data, where the model formulations varied by the thematic scale  
 334 and classification scheme (row), addition of covariates (fill) and satellite used for the satellite  
 335 imagery (colour).



336

337 Figure 3. The sensitivity for each ecosystem class (panels) as an exemplar by-class evaluation  
 338 metric for the different classification schemes (shape), covariates used (fill), and satellite used  
 339 for the imagery (colour),. Ecosystem types that were grouped when the classification scheme  
 340 changed into ecosystem functional groups (EFGs, shape: circle, panel title colour: light grey box)  
 341 and biomes (shape: triangle, panel title colour: dark grey box) are identified by an x. Sensitivity  
 342 is the ability of the model to correctly predict the true class from all those known to be true in  
 343 the reference points.

344 The satellite from which the satellite image was acquired was the second most influential  
345 modelling decision. The models that used the Landsat-9 satellite image achieved higher overall  
346 accuracy than those models using the Sentinel-2 image (Figure 2, and Appendix S6). The effect  
347 of the satellite was most pronounced when only the satellite-image covariates were used. With  
348 additional covariates, the Landsat-9 satellite image still improved model performance, although  
349 to a lesser degree (Figure 2). Landsat-9 also produced high by-class accuracies; however, the  
350 effect varied (Figure 3). For example, the *dry* and *wet rainforests* showed by-class  
351 improvements with images acquired from the Sentinel-2 satellite (Figure 3, and Appendix S6).

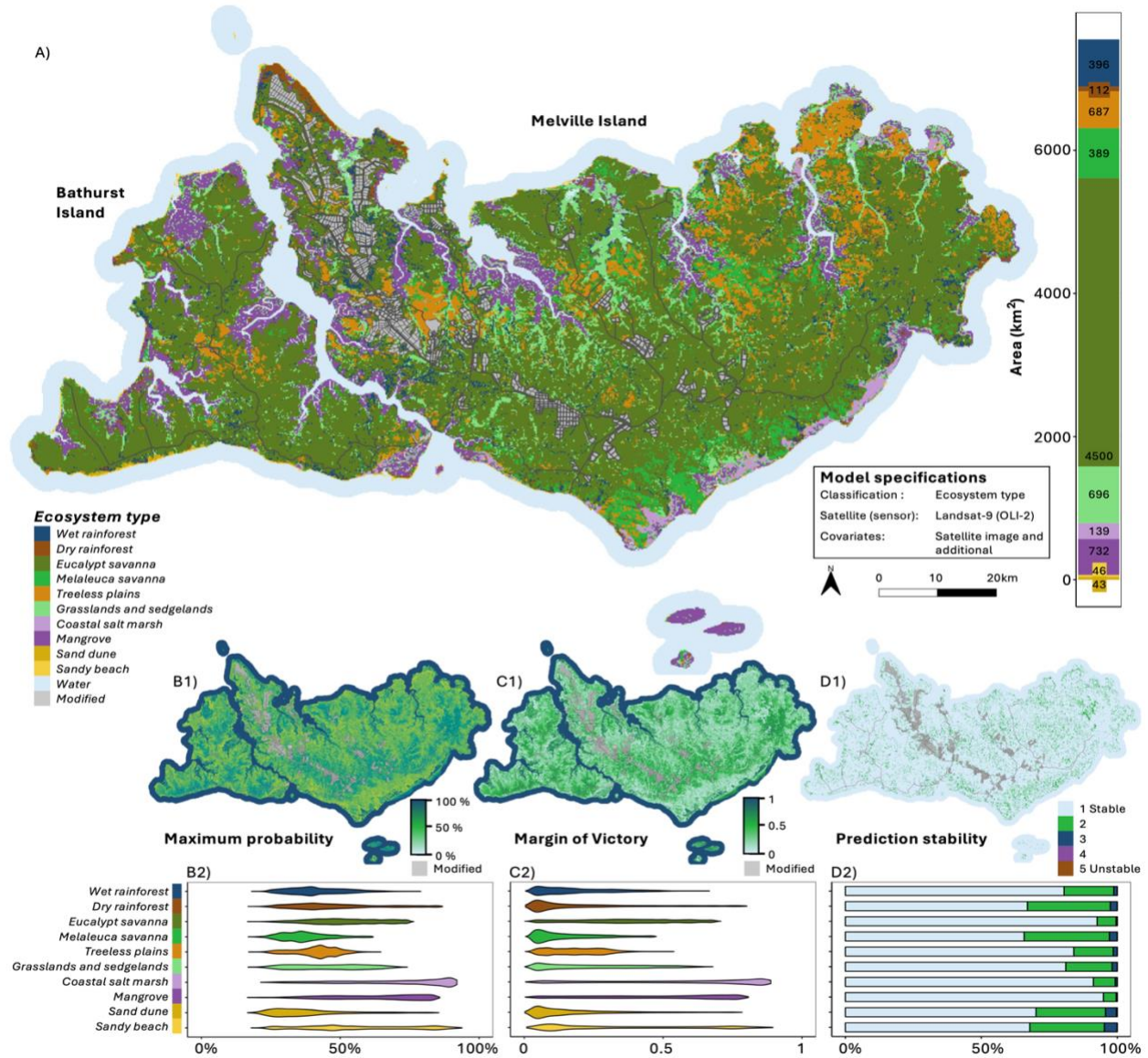
352

353 The classification scheme was the least impactful modelling decision that we tested on the  
354 evaluation metrics. The biome classes (the coarsest grouping) slightly improved the overall  
355 evaluation metrics, compared to the ecosystem and ecosystem functional groups (Figure 2).  
356 This effect was less pronounced with the combined satellite and additional covariates, and for  
357 images acquired from the Sentinel-2 satellite (Figure 2, and Appendix S6). In general, the biome  
358 classification scheme did not change the by-class evaluation estimates (Figure 3), the exception  
359 being the *wet* and *dry rainforest* ecosystem types which were often misclassified in other  
360 classification schemes (Appendix S6).

361

362 The maximum probability and MoV maps imply similar patterns of prediction confidence  
363 (Figure 4.B1 and C1). Areas with high confidence occur in a central band and eastern patch on  
364 Melville Island, and in isolated areas of Bathurst Island. Low confidence areas, including low  
365 stability in the prediction (Figure 4.D1), are scattered across the landscape with an aggregation

366 on the southern coast and far east area of Melville Island. Summarising the prediction  
367 confidence across the entire area (Figure 4.B2-D2), the *coastal salt marsh* (light purple) and  
368 *mangrove* (dark purple) were predicted with highest confidence (median maximum probability  
369 = 75.72% and 64.77%, respectively, and median MoV = 66.15% and 50.46%), indicated by the  
370 distribution of the maximum probability and MoV skewed to the right (Figure 4.B2-C2).  
371 *Mangroves* were also the most stable ecosystem type with 94.86% of the cells mapped as  
372 mangroves only ever predicted to be mangroves, followed by *eucalypt savanna* at 92.57%  
373 (Figure 4.D2, light blue boxes). *Sand dunes* were predicted with the low maximum probability  
374 values (median of 34.82%) indicated by the distribution skewed to the left (Figure 4.B2, dark  
375 yellow), while the MoV distribution is low (median of 11.89%) but comparable to other classes  
376 (Figure 4.C2). *Sand dunes* and *sandy beaches* produced unstable predictions with the highest  
377 proportion of cells predicted as three different classes (4.65% and 4.03%, Figure 4.D2 dark blue  
378 bar), followed by *melaleuca savanna* and *dry rainforests* with the highest proportion of cells  
379 with two classes (31.35% and 30.46%, Figure 4.D2 green bar).



380  
 381 Figure 4. Ecosystem distributions on the Tiwi Islands, Australia and the remaining uncertainty as  
 382 maps (b1-d2) and distributions for each class (b2-d2) for an example model using the  
 383 ecosystem type classes, Landsat-9 satellite imagery, and additional covariates alongside those  
 384 from the satellite image. For b2 and c2, the values are the mean of the cross-validation models  
 385 and the colours correspond to the ecosystem type. The colours for d1 and d2 correspond to the  
 386 number of possible ecosystem classes predicted across the five cross-validation folds.

387

388 **4. Discussion**

389 Decisions made during modelling strongly impacted ecosystem map accuracy and outputs  
390 (Figure 2 and Figure 3). Incorporating additional covariates alongside a satellite image improved  
391 overall model performance and many per-class metrics, supporting previous calls to ground  
392 ecosystem model development in ecological theory and with domain expertise (Xiao *et al.*,  
393 2024). As choice of satellite and classification scheme were less influential, other considerations  
394 can guide the decision. The extensive Landsat archive facilitates change mapping, while finer  
395 thematic classification preserves information relevant for biodiversity management.

396

397 Ecological theory posits that the distribution of biodiversity is shaped by environmental  
398 gradients. Unsurprisingly, our results showed that the best predictions came from a model with  
399 a greater number and diversity of covariates upon which it could separate the ecosystem  
400 classes. This result aligns with previous research (Venter and Sydenham, 2021; Simensen *et al.*,  
401 2020; Trouvé *et al.*, 2023; Naas *et al.*, 2024). Predictions for the *treeless plains* ecosystem  
402 greatly improved with the additional covariates. This ecosystems frequently misclassified as  
403 *Melaleuca savanna*, potentially due the varied dominant species and structural formations of  
404 the *treeless plains* (Wilson and Fensham, 1994) and presence of *Melaleuca viridiflora* co-  
405 dominant in the canopy producing a variable spectral signature that overlaps with that of  
406 *Melaleuca savanna*. Additional variables instead allowed for the model to resolve these  
407 environmental niches. Elevation contributed the most explanatory power across the  
408 ecosystems (Appendix 2.6), likely acting as a proxy for other ecological gradients and processes  
409 (Whittaker, 1956). Topographic covariates representing water availability are valuable to  
410 distinguish wet and dry forest types, such as rainforests and riparian forests (Trouvé *et al.*,  
411 2023). In other regions where water availability is not a dominant driver of ecosystem  
412 distributions, other covariates may provide greater explanatory power. When maps are  
413 developed at national scales and span a range of latitudes, climate variables capturing  
414 temperature and rainfall patterns will become increasingly useful, as seen in Korea (Lee *et al.*,  
415 2025). Producers of maps should carefully consider the ecosystems they are modelling, and  
416 choose relevant covariates for the region.

417

418 The usefulness of the covariates to explain ecological patterns is constrained by the covariate  
419 quality and accuracy. Soil covariates were the least informative in this study (Appendix 2.6),  
420 potentially due to the coarse spatial resolution or underlying data inaccuracies in the available  
421 dataset noted in other global and national soil maps (Rossiter *et al.*, 2022; Maynard *et al.*,  
422 2023), rather than a lack of ecological importance (Simensen *et al.*, 2020; Keith *et al.*, 2022).  
423 Improving the availability, accessibility, and spatiotemporal resolution of ecological covariates  
424 would improve both map accuracy and our understanding of the environmental gradients  
425 defining their extent.

426

427 While the additional covariates contributed useful information, we found that the satellite  
428 covariates remained highly informative (Appendix 2.6), consistent with findings that ecological  
429 or climate covariates perform best alongside, rather than instead of, satellite imagery  
430 (Simensen *et al.*, 2020; Trouvé *et al.*, 2023; Naas *et al.*, 2024). We observed that satellite image  
431 covariates performed well for specific ecosystems, namely the *coastal salt marsh*, *sandy beach*  
432 shorelines, and *water*. The value of investing in additional covariates varies by ecosystem.  
433 Producers should weigh expected performance gains against the time and cost of data  
434 acquisition. Comparison of additional covariates including radar data, texture metrics, and  
435 temporal signals related to phenology will be a valuable area for future research.

436

437 In addition to the model covariates, we found that the Landsat-9 satellite imagery  
438 outperformed Sentinel-2 data overall (Figure 2) and for individual classes (Figure 3), although  
439 the effect lessened with the inclusion of additional covariates. Exceptions to this were the dry  
440 rainforest ecosystem types, potentially because the spatial resolution imagery better detected  
441 the sharp boundaries that delineate rainforests, reducing the number of pixels containing  
442 multiple ecosystem types. These mixed pixels are a high source of uncertainty in landcover  
443 mapping (Loosvelt *et al.*, 2012) and hamper the reliability of global and national maps (Herold  
444 *et al.*, 2008; Congalton *et al.*, 2014). Alternatively, high spatial resolution sensors may detect  
445 structural variability within ecosystem classes leading to high intra-class variability and noise  
446 (Nagendra and Rocchini, 2008; Rocchini *et al.*, 2013). For instance, savanna ecosystems display  
447 highly variable tree occurrence and canopy cover (Keith *et al.*, 2022) while sand dunes are a  
448 mosaic of vegetated and unvegetated areas (Young *et al.*, 2025), potentially explaining why  
449 Landsat-9 generally performed better for these ecosystems (Figure 3). While here we have  
450 described the potential effect of spatial resolution, we cannot disentangle this effect from the  
451 other differences between the missions such as the return time and spectral resolution  
452 (Pettorelli *et al.*, 2014; Phiri *et al.*, 2020). Across the literature, satellite spatial resolution has no  
453 consistent effect on map accuracy (Yu *et al.*, 2014; Morales-Barquero *et al.*, 2019). Satellite  
454 selection should therefore be guided by management objectives, ecosystem characteristics,  
455 and regional context (Horvath *et al.*, 2021; Venter *et al.*, 2022; Liu *et al.*, 2023; Naas *et al.*,  
456 2024). The additional benefit of the Landsat satellites is the rich archive of images (Wulder *et*  
457 *al.*, 2012) and hence the potential to detect historical changes (Murray *et al.*, 2019; Calderón-

458 Loor, Hadjikakou and Bryan, 2021), whereas satellites with shorter revisit times may be better  
459 for cloudy regions (Liu *et al.*, 2023).

460

461 The least influential modelling decision was the classification scheme. Overall evaluation  
462 metrics slightly improved with the GET level 2 ‘biome’ scale representing the fewest classes and  
463 coarsest scale of biodiversity. Aggregating classes is a common method to improve accuracy  
464 (Congalton and Green, 1993; Rempel, 2009) but, overall, the benefits are small and variable (Yu  
465 *et al.*, 2014). Importantly, modelling biomes presents a direct trade-off with usefulness for  
466 downstream ecological applications. The improvements we observed were driven by  
467 aggregating specific classes that were often misclassified, namely the wet and dry rainforest.  
468 These two rainforest ecosystems are classified into the same ‘tropical and subtropical forests  
469 biome’ but globally differ in threat (Etter *et al.*, 2017; Murray *et al.*, 2020; Noh *et al.*, 2020) and  
470 protection status (Wohlfart, Wegmann and Leimgruber, 2014; Rivas, Guerrero-Casado and  
471 Navarro-Cerillo, 2021). Aggregating and mapping these ecosystems as a single biome obscures  
472 the urgency and practicality of protecting and managing the world’s tropical forests.

473

474 Thoughtful model formulation can reduce but never remove uncertainty in maps (Rocchini *et*  
475 *al.*, 2013; Foody, 2021). As demonstrated here, uncertainty maps are immediate tools that can  
476 be readily implemented to communicate spatial patterns of uncertainty and to facilitate  
477 inclusion in downstream applications. Emerging methods offer rigorous uncertainty  
478 quantitation, such as conformal predictions, as ecosystem mapping adopts novel and complex

479 models, methods for quantifying and communicating spatial uncertainty will need to continue  
480 to develop, rendering this an important area for future research.

481  
482 Uncertainty maps also offer a practical function to map improvement by directing future data  
483 collection. Used alongside by-class evaluation metrics, data collection efforts can target poor  
484 performing classes, those with few reference points, as well as in geographical areas with high  
485 uncertainty. Iterating on ecosystem maps through data collection and validation with local  
486 expertise is a crucial pathway to improve map accuracy, alongside additional benefits for result  
487 uptake and ... (ref Falko and Mandy guidelines). Continued iteration will further improve map  
488 accuracy and reduce uncertainty, thereby strengthening the evidence base for conservation.

489

## 490 Conclusion

491 Modelling decisions shape ecosystem maps. As ecosystem mapping scales up to meet broad-  
492 scale monitoring and international conservation commitments (Galaz García *et al.*, 2023;  
493 Pettorelli *et al.*, 2024), the rigor of testing model decisions must improve. Uncertainty is an  
494 inherent feature of ecosystem maps, rather than a failure of the model. Map producers have a  
495 responsibility to communicate map reliability, through transparent reporting of decisions,  
496 evaluation metrics, and uncertainty maps. Map users should propagate known uncertainties  
497 into downstream applications.

## 498 **Acknowledgements**

499 We acknowledge the extensive work undertaken by previous researchers, consultants, and  
500 industry professionals in developing their respective datasets and products which allowed the  
501 creation of the reference points for this research. The Tiwi Islands are the lands of the Tiwi  
502 people from eight land-owning clans: Jikilaruwu, Malawu, Mantiyupwi, Marrikawuyanga,  
503 Munupi, Wulirankuwu, Wurankuwu, and Yimpinari. We would like to thank Mavis Kerinauia,  
504 Colin Kerinauia, Simon Munkara, Bernard Tipoloura, Gemma Munkara, John Louis Munkara,  
505 Kinjia Munkara-Murray and Marie Munkara for visiting locations on the Tiwi Islands. We thank  
506 Mavis Kerinariaua, Alana Brekelmans, Margaret Ayre, Michaela Spencer, the Tiwi Land Council,  
507 Tiwi Resources, and Tiwi rangers for their involvement and facilitation during on-ground visits.  
508 Analysis and writing were undertaken on the lands of the Wurundjeri Woi Wurung peoples of  
509 the Kulin Nation. This research was funded by the Australian Research Council (ARC) linkage  
510 grant (LP170100305) in partnership with the Tiwi Land Council. The fieldwork with Tiwi People  
511 was funded by the Foundation for National Parks and Wildlife community conservation grant  
512 (FNPW028CCG22). Human ethics was approved by The University of Melbourne Human Ethics  
513 (#1955248) and Deakin University Human Research Ethics Committee (#2022097). Permission  
514 to enter the Tiwi Islands was granted for each trip by the Tiwi Land Council.

515

516 **Funding statement:**

517 This research was funded by the Australian Research Council (ARC) linkage grant (LP170100305)  
518 in partnership with the Tiwi Land Council. The fieldwork with Tiwi People was funded by the  
519 Foundation for National Parks and Wildlife community conservation grant (FNPW028CCG22).

520

521 **Ethics approval statement:**

522 Human ethics was approved by The University of Melbourne Human Ethics (#1955248) and

523 Deakin University Human Research Ethics Committee (#2022097). Permission to enter the Tiwi

524 Islands was granted for each trip by the Tiwi Land Council.

## 525 References

- 526 Aybar, C., Wu, Q., Bautista, L., Yali, R. and Barja, A. (2020) 'rgee: An R package for interacting with Google Earth Engine', *Journal of Open Source*  
527 *Software*, 5(51), p. 2272. Available at: <https://doi.org/10.21105/joss.02272>.
- 528 Barry, S. and Elith, J. (2006) 'Error and uncertainty in habitat models', *Journal of Applied Ecology*, 43(3), pp. 413–423. Available at:  
529 <https://doi.org/10.1111/j.1365-2664.2006.01136.x>.
- 530 Brocklehurst, P. and Lynch, B. (2009) *Northern Territory Melaleuca forest survey*. Technical Report 25/2009D. Palmerston, Northern Territory:  
531 Department of Natural Resources, Environment, The Arts and Sport.
- 532 Brocklehurst, P. and Lynch, D. (2001) *Melaleuca Survey of the Top End, Northern Territory*. Technical Report 25/2009D. Palmerston, Northern  
533 Territory: Department of Natural Resources, Environment, The Arts and Sport, p. 89.
- 534 Burgman, M.A., Lindenmayer, D.B. and Elith, J. (2005) 'Managing Landscapes for Conservation Under Uncertainty', *Ecology*, 86(8), pp. 2007–  
535 2017. Available at: <https://doi.org/10.1890/04-0906>.
- 536 Calderón-Loor, M., Hadjikakou, M. and Bryan, B.A. (2021) 'High-resolution wall-to-wall land-cover mapping and land change assessment for  
537 Australia from 1985 to 2015', *Remote Sensing of Environment*, 252, p. 112148. Available at: <https://doi.org/10.1016/j.rse.2020.112148>.
- 538 Capotorti, G., Del Vico, E., Copiz, R., Facioni, L., Zavattero, L., Bonacquisti, S., Paolanti, M. and Blasi, C. (2023) 'Ecosystems of Italy. Updated  
539 mapping and typology for the implementation of national and international biodiversity-related policies', *Plant Biosystems - An International*  
540 *Journal Dealing with all Aspects of Plant Biology*, 157(6), pp. 1248–1258. Available at: <https://doi.org/10.1080/11263504.2023.2284135>.
- 541 CBD (1992) *Convention on biological diversity*. Rio de Janeiro: United Nations. Available at:  
542 [https://treaties.un.org/doc/Treaties/1992/06/19920605%2008-44%20PM/Ch\\_XXVII\\_08p.pdf](https://treaties.un.org/doc/Treaties/1992/06/19920605%2008-44%20PM/Ch_XXVII_08p.pdf).
- 543 Congalton, R.G. and Green, K. (1993) 'A practical look at the sources of confusion in error matrix generation.', *Photogrammetric engineering*  
544 *and remote sensing*, 59(5), pp. 641–644.
- 545 Congalton, R.G., Gu, J., Yadav, K., Thenkabail, P. and Ozdogan, M. (2014) 'Global Land Cover Mapping: A Review and Uncertainty Analysis',  
546 *Remote Sensing*, 6(12), pp. 12070–12093. Available at: <https://doi.org/10.3390/rs61212070>.
- 547 Davies, H.F., McCarthy, M.A., Firth, R.S.C., Woinarski, J.C.Z., Gillespie, G.R., Andersen, A.N., Rioli, W., Puruntatameri, J., Roberts, W., Kerinauia,  
548 C., Kerinauia, V., Womatakimi, K.B. and Murphy, B.P. (2018) 'Declining populations in one of the last refuges for threatened mammal species in  
549 northern Australia', *Austral Ecology*, 43(5), pp. 602–612. Available at: <https://doi.org/10.1111/aec.12596>.
- 550 Davies, H.F., Rangers, T.L., Rees, M.W., Stokeld, D., Miller, A.C., Gillespie, G.R. and Murphy, B.P. (2021) 'Variation in feral cat density between  
551 two large adjacent islands in Australia's monsoon tropics', *Pacific Conservation Biology*, 28(1), pp. 18–24. Available at:  
552 <https://doi.org/10.1071/PC20088>.
- 553 Davies, H.F., Rioli, W., Puruntatameri, J., Roberts, W., Kerinauia, C., Kerinauia, V., Womatakimi, K.B., Gillespie, G.R. and Murphy, B.P. (2019)  
554 'Estimating site occupancy and detectability of the threatened partridge pigeon (*Geophaps smithii*) using camera traps', *Austral Ecology*, 44(5),  
555 pp. 868–879. Available at: <https://doi.org/10.1111/aec.12755>.
- 556 DCCEEW (2021) 'Interim Biogeographic Regionalisation for Australia (IBRA)'.
- 557 De la Cruz, M., Quintana-Ascencio, P.F., Cayuela, L., Espinosa, C.I. and Escudero, A. (2017) 'Comment on "The extent of forest in dryland  
558 biomes"', *Science* [Preprint]. Available at: <https://doi.org/10.1126/science.aao0369>.
- 559 Dormann, C.F., Elith, J., Bacher, S., Buchmann, C., Carl, G., Carré, G., Marquéz, J.R.G., Gruber, B., Lafourcade, B., Leitão, P.J., Münkemüller, T.,  
560 McClean, C., Osborne, P.E., Reineking, B., Schröder, B., Skidmore, A.K., Zurell, D. and Lautenbach, S. (2013) 'Collinearity: a review of methods to  
561 deal with it and a simulation study evaluating their performance', *Ecography*, 36(1), pp. 27–46. Available at: <https://doi.org/10.1111/j.1600-0587.2012.07348.x>.
- 563 Dorrrough, J., Tozer, M., Armstrong, R., Summerell, G. and Scott, M.L. (2021) 'Quantifying uncertainty in the identification of endangered  
564 ecological communities', *Conservation Science and Practice*, 3(11), p. e537. Available at: <https://doi.org/10.1111/csp2.537>.
- 565 Dryflor, Banda-R, K., Delgado-Salinas, A., Dexter, K.G., Linares-Palomino, R., Oliveira-Filho, A., Prado, D., Pullan, M., Quintana, C., Riina, R.,  
566 Rodríguez M., G.M., Weintritt, J., Acevedo-Rodríguez, P., Adarve, J., Álvarez, E., Aranguren B., A., Arteaga, J.C., Aymard, G., Castaño, A.,  
567 Ceballos-Mago, N., Cogollo, Á., Cuadros, H., Delgado, F., Devia, W., Dueñas, H., Fajardo, L., Fernández, Á., Fernández, M.Á., Franklin, J., Freid,

- 568 E.H., Galetti, L.A., Gonto, R., González-M., R., Graveson, R., Helmer, E.H., Idárraga, Á., López, R., Marcano-Vega, H., Martínez, O.G., Maturo,  
569 H.M., McDonald, M., McLaren, K., Melo, O., Mijares, F., Mogni, V., Molina, D., Moreno, N.D.P., Nassar, J.M., Neves, D.M., Oakley, L.J., Oatham,  
570 M., Olvera-Luna, A.R., Pezzini, F.F., Dominguez, O.J.R., Ríos, M.E., Rivera, O., Rodríguez, N., Rojas, A., Särkinen, T., Sánchez, R., Smith, M., Vargas,  
571 C., Villanueva, B. and Pennington, R.T. (2016) 'Plant diversity patterns in neotropical dry forests and their conservation implications', *Science*,  
572 353(6306), pp. 1383–1387. Available at: <https://doi.org/10.1126/science.aaf5080>.
- 573 EcOz Environmental Consultants (2021) *Terrestrial Ecology Report - Tiwi Islands H2 Project. Provaris Energy*. Report for Provaris Energy. Darwin,  
574 Northern Territory.
- 575 EcOz Environmental Services (2012) *Kilimiraka Notice of Intent: Kilimiraka Mineral Sands Project, Bathurst Island, N.T.* Report for Matilda Zircon.
- 576 Elith, J., Burgman, M.A. and Regan, H.M. (2002) 'Mapping epistemic uncertainties and vague concepts in predictions of species distribution',  
577 *Ecological Modelling*, 157(2), pp. 313–329. Available at: [https://doi.org/10.1016/S0304-3800\(02\)00202-8](https://doi.org/10.1016/S0304-3800(02)00202-8).
- 578 Etter, A., Andrade, Á., Saavedra, K., Amaya, P. and Arévalo, P. (2017) *Estado de los Ecosistemas Colombianos: una aplicación de la metodología*  
579 *de la Lista Roja de Ecosistemas (Vers.2.0)*. Bogota, Colombia: Pontificia Universidad Javeriana y Conservación Internacional Colombia, p. 138.  
580 Available at: [https://www.conservation.org.co/media/A7.LRE-Colombia\\_INFORME%20FINAL\\_%202017.pdf](https://www.conservation.org.co/media/A7.LRE-Colombia_INFORME%20FINAL_%202017.pdf).
- 581 Foody, G.M. (2002) 'Status of land cover classification accuracy assessment', *Remote Sensing of Environment*, 80(1), pp. 185–201. Available at:  
582 [https://doi.org/10.1016/S0034-4257\(01\)00295-4](https://doi.org/10.1016/S0034-4257(01)00295-4).
- 583 Foody, G.M. (2020) 'Explaining the unsuitability of the kappa coefficient in the assessment and comparison of the accuracy of thematic maps  
584 obtained by image classification', *Remote Sensing of Environment*, 239, p. 111630. Available at: <https://doi.org/10.1016/j.rse.2019.111630>.
- 585 Foody, G.M. (2021) 'Impacts of ignorance on the accuracy of image classification and thematic mapping', *Remote Sensing of Environment*, 259,  
586 p. 112367. Available at: <https://doi.org/10.1016/j.rse.2021.112367>.
- 587 Foody, G.M. (2022) 'Global and Local Assessment of Image Classification Quality on an Overall and Per-Class Basis without Ground Reference  
588 Data', *Remote Sensing*, 14(21), p. 5380. Available at: <https://doi.org/10.3390/rs14215380>.
- 589 Galaz García, C., Bagstad, K.J., Brun, J., Chaplin-Kramer, R., Dhu, T., Murray, N.J., Nolan, C.J., Ricketts, T.H., Sosik, H.M., Sousa, D., Willard, G. and  
590 Halpern, B.S. (2023) 'The future of ecosystem assessments is automation, collaboration, and artificial intelligence', *Environmental Research*  
591 *Letters*, 18(1), p. 011003. Available at: <https://doi.org/10.1088/1748-9326/acab19>.
- 592 Gallant, J., Wilson, N., Tickle, P.K., Downling, T. and Read, A. (2009) '3 second SRTM Derived Digital Elevation Model (DEM) Version 1.0.'  
593 Canberra: Geoscience Australia. Available at: <http://pid.geoscience.gov.au/dataset/ga/69888>.
- 594 Gambold, N. and Woinarski, J.C.Z. (1993) 'Distributional patterns of herpetofauna in monsoon rainforests of the Northern Territory, Australia',  
595 *Australian Journal of Ecology*, 18(4), pp. 431–449. Available at: <https://doi.org/10.1111/j.1442-9993.1993.tb00470.x>.
- 596 Gorelick, N., Hancher, M., Dixon, M., Ilyushchenko, S., Thau, D. and Moore, R. (2017) 'Google Earth Engine: Planetary-scale geospatial analysis  
597 for everyone', *Remote Sensing of Environment*, 202, pp. 18–27. Available at: <https://doi.org/10.1016/j.rse.2017.06.031>.
- 598 Gould, E., Fraser, H.S., Parker, T.H., Nakagawa, S., Griffith, S.C., Vesik, P.A., Fidler, F., Hamilton, D.G., Abbey-Lee, R.N., Abbott, J.K., Aguirre, L.A.,  
599 Alcaraz, C., Aloni, I., Altschul, D., Arekar, K., Atkins, J.W., Atkinson, J., Baker, C., Barrett, M., Bell, K., Bello, S.K., Beltrán, I., Berauer, B.J., Bertram,  
600 M.G., Billman, P.D., Blake, C.K., Blake, S., Bliard, L., Bonisoli-Alquati, A., Bonnet, T., Bordes, C.N.M., Bose, A.P.H., Botterill-James, T., Boyd, M.A.,  
601 Boyle, S.A., Bradfer-Lawrence, T., Bradham, J., Brand, J.A., Brengdahl, M.I., Bulla, M., Bussière, L., Camerlenghi, E., Campbell, S.E., Campos,  
602 L.L.F., Caravaggi, A., Cardoso, P., Carroll, C.J.W., Catanach, T.A., Chen, X., Chik, H.Y.J., Choy, E.S., Christie, A.P., Chuang, A., Chunco, A.J., Clark,  
603 B.L., Contina, A., Covernton, G.A., Cox, M.P., Cressman, K.A., Crotti, M., Crouch, C.D., D'Amelio, P.B., Sousa, A.A. de, Döbert, T.F., Dobler, R.,  
604 Dobson, A.J., Doherty, T.S., Drobniak, S.M., Duffy, A.G., Duncan, A.B., Dunn, R.P., Dunning, J., Dutta, T., Eberhart-Hertel, L., Elmore, J.A., Elsherif,  
605 M.M., English, H.M., Ensminger, D.C., Ernst, U.R., Ferguson, S.M., Fernández-Juricic, E., Ferreira-Arruda, T., Fieberg, J., Finch, E.A., Fiorenza, E.A.,  
606 Fisher, D.N., Fontaine, A., Forstmeier, W., Fourcade, Y., Frank, G.S., Freund, C.A., Fuentes-Lillo, E., Gandy, S.L., Gannon, D.G., García-Cervigón,  
607 A.I., Garretson, A.C., Ge, X., Geary, W.L., Géron, C., Gilles, M., Girndt, A., Gliksmán, D., Goldspiel, H.B., Gomes, D.G.E., Good, M.K., Goslee, S.C.,  
608 Gosnell, J.S., Grames, E.M., Gratton, P., Grebe, N.M., Greenler, S.M., Griffioen, M., Griffith, D.M., Griffith, F.J., Grossman, J.J., Güncan, A.,  
609 Haesen, S., Hagan, J.G., Hager, H.A., Harris, J.P., Harrison, N.D., Hasnain, S.S., Havird, J.C., Heaton, A.J., Herrera-Chaustre, M.L., Howard, T.J.,  
610 Hsu, B.-Y., Iannarilli, F., Iranzo, E.C., Iverson, E.N.K., Jimoh, S.O., Johnson, D.H., Johnsson, M., Jorna, J., Jucker, T., Jung, M., Kačergytė, I., Kaltz,  
611 O., Ke, A., Kelly, C.D., Keogan, K., Keppeler, F.W., Killion, A.K., Kim, D., Kochan, D.P., Korsten, P., Kothari, S., Kuppler, J., Kusch, J.M., Lagisz, M.,  
612 Lalla, K.M., Larkin, D.J., Larson, C.L., Lauck, K.S., Lauterbur, M.E., Law, A., Léandri-Breton, D.-J., Lembrechts, J.J., L'Herpinier, K., Lievens, E.J.P.,  
613 Lima, D.O. de, Lindsay, S., Luquet, M., MacLeod, R., Macphie, K.H., Magellan, K., Mair, M.M., Malm, L.E., Mammola, S., Mandeville, C.P.,  
614 Manhart, M., Manrique-Garzon, L.M., Mäntylä, E., Marchand, P., Marshall, B.M., Martin, C.A., Martin, D.A., Martin, J.M., Martinig, A.R.,  
615 McCallum, E.S., McCauley, M., McNew, S.M., Meiners, S.J., Merklung, T., Michelangeli, M., Moiron, M., Moreira, B., Mortensen, J., Mos, B.,  
616 Muraina, T.O., Murphy, P.W., Nelli, L., Niemelä, P., Nightingale, J., Nilsson, G., Nolzaco, S., Nooten, S.S., Novotny, J.L., Olin, A.B., Organ, C.L.,  
617 Ostevik, K.L., Palacio, F.X., Paquet, M., Parker, D.J., Pascall, D.J., Pasquarella, V.J., Paterson, J.H., Payo-Payo, A., Pedersen, K.M., Perez, G., Perry,

- 618 K.I., Pottier, P., Proulx, M.J., Proulx, R., Pruett, J.L., Ramananjato, V., Randimbiarison, F.T., Razafindratsima, O.H., Rennison, D.J., Riva, F., Riyahi,  
619 S., Roast, M.J., Rocha, F.P., Roche, D.G., Román-Palacios, C., Rosenberg, M.S., Ross, J., Rowland, F.E., Rugemalila, D., Russell, A.L., Ruuskanen, S.,  
620 Saccone, P., Sadeh, A., Salazar, S.M., Sales, K., Salmón, P., Sánchez-Tójar, A., Santos, L.P., Santostefano, F., Schilling, H.T., Schmidt, M., Schmoll,  
621 T., Schneider, A.C., Schrock, A.E., Schroeder, J., Schtickzelle, N., Schultz, N.L., Scott, D.A., Scroggie, M.P., Shapiro, J.T., Sharma, N., Shearer, C.L.,  
622 Simón, D., Sitvarin, M.I., Skupien, F.L., Slinn, H.L., Smith, G.P., Smith, J.A., Sollmann, R., Whitney, K.S., Still, S.M., Stuber, E.F., Sutton, G.F.,  
623 Swallow, B., Taff, C.C., Takola, E., Tanentzap, A.J., Tarjuelo, R., Telford, R.J., Thawley, C.J., Thierry, H., Thomson, J., Tidau, S., Tompkins, E.M.,  
624 Tortorelli, C.M., Trlica, A., Turnell, B.R., Urban, L., Vondel, S.V. de, Wal, J.E.M. van der, Eekhoven, J.V., Oordt, F. van, Vanderwel, K.M.,  
625 Vanderwel, M.C., Vanderwolf, K.J., Vélez, J., Vergara-Florez, D.C., Verrelli, B.C., Vieira, M.V., Villamil, N., Vitali, V., Vollering, J., Walker, J.,  
626 Walker, X.J., Walter, J.A., Waryszak, P., Weaver, R.J., Wedegärtner, R.E.M., Weller, D.L., Whelan, S., White, R.L., Wolfson, D.W., Wood, A.,  
627 Yanco, S.W., Yen, J.D.L., Youngflesh, C., Zilio, G., Zimmer, C., Zimmerman, G.M. and Zitomer, R.A. (2023) 'Same data, different analysts: variation  
628 in effect sizes due to analytical decisions in ecology and evolutionary biology'. Available at:  
629 [https://ecoevorxiv.org/repository/view/6000/?utm\\_source=miragenews&utm\\_medium=miragenews&utm\\_campaign=news](https://ecoevorxiv.org/repository/view/6000/?utm_source=miragenews&utm_medium=miragenews&utm_campaign=news) (Accessed: 1  
630 August 2024).
- 631 Grimmett, L., Whitsed, R. and Horta, A. (2020) 'Presence-only species distribution models are sensitive to sample prevalence: Evaluating models  
632 using spatial prediction stability and accuracy metrics', *Ecological Modelling*, 431, p. 109194. Available at:  
633 <https://doi.org/10.1016/j.ecolmodel.2020.109194>.
- 634 Hein, L., Bagstad, K.J., Obst, C., Edens, B., Schenau, S., Castillo, G., Soulard, F., Brown, C., Driver, A., Bordt, M., Steurer, A., Harris, R. and  
635 Caparrós, A. (2020) 'Progress in natural capital accounting for ecosystems', *Science*, 367(6477), pp. 514–515. Available at:  
636 <https://doi.org/10.1126/science.aaz8901>.
- 637 Herold, M., Mayaux, P., Woodcock, C.E., Baccini, A. and Schmullius, C. (2008) 'Some challenges in global land cover mapping: An assessment of  
638 agreement and accuracy in existing 1 km datasets', *Remote Sensing of Environment*, 112(5), pp. 2538–2556. Available at:  
639 <https://doi.org/10.1016/j.rse.2007.11.013>.
- 640 Hijmans, R.J. (2023) 'terra: Spatial Data Analysis'. Available at: <https://CRAN.R-project.org/package=terra>.
- 641 Horvath, P., Halvorsen, R., Simensen, T. and Bryn, A. (2021) 'A comparison of three ways to assemble wall-to-wall maps from distribution  
642 models of vegetation types', *GIScience & Remote Sensing*, 58(8), pp. 1458–1476. Available at:  
643 <https://doi.org/10.1080/15481603.2021.1996313>.
- 644 Jansen, J., Woolley, S.N.C., Dunstan, P.K., Foster, S.D., Hill, N.A., Haward, M. and Johnson, C.R. (2022) 'Stop ignoring map uncertainty in  
645 biodiversity science and conservation policy', *Nature Ecology & Evolution*, 6(7), pp. 828–829. Available at: <https://doi.org/10.1038/s41559-022-01778-z>.  
646
- 647 Keith, D.A., Ferrer-Paris, J.R., Ghoraba, S.M.M., Henriksen, S., Monyeki, M., Murray, N.J., Nicholson, E., Rowland, J.A., Skowno, A., Slingsby, J.A.,  
648 Storeng, A.B., Valderrábano, M. and Zager, I. (eds) (2024) *Guidelines for the application of IUCN Red List of ecosystems categories and criteria*  
649 *version 2*. IUCN International Union for Conservation of Nature. Available at: <https://doi.org/10.2305/IUCN.CH.2016.RLE.1.en>.
- 650 Keith, D.A., Ferrer-Paris, J.R., Nicholson, E., Bishop, M.J., Polidoro, B.A., Ramirez-Llodra, E., Tozer, M.G., Nel, J.L., Mac Nally, R., Gregr, E.J.,  
651 Watermeyer, K.E., Essl, F., Faber-Langendoen, D., Franklin, J., Lehmann, C.E.R., Etter, A., Roux, D.J., Stark, J.S., Rowland, J.A., Brummitt, N.A.,  
652 Fernandez-Arcaya, U.C., Suthers, I.M., Wiser, S.K., Donohue, I., Jackson, L.J., Pennington, R.T., Iliffe, T.M., Gerovasileiou, V., Giller, P., Robson,  
653 B.J., Pettorelli, N., Andrade, A., Lindgaard, A., Tahvanainen, T., Terauds, A., Chadwick, M.A., Murray, N.J., Moat, J., Plissock, P., Zager, I. and  
654 Kingsford, R.T. (2022) 'A function-based typology for Earth's ecosystems', *Nature*, 610(7932), pp. 513–518. Available at:  
655 <https://doi.org/10.1038/s41586-022-05318-4>.
- 656 Keith, D.A., Ghoraba, S.M.M., Kaly, E., Jones, K.R., Oosthuizen, A., Obura, D., Costa, H.M., Daniels, F., Duarte, E., Grantham, H., Gudka, M.,  
657 Norman, J., Shannon, L.J., Skowno, A. and Ferrer-Paris, J.R. (2024) 'Contributions of the IUCN Red List of Ecosystems to risk-based design and  
658 management of protected and conserved areas in Africa', *Conservation Biology*, 38(3), p. e14169. Available at:  
659 <https://doi.org/10.1111/cobi.14169>.
- 660 Khatami, R., Mountrakis, G. and Stehman, S.V. (2016) 'A meta-analysis of remote sensing research on supervised pixel-based land-cover image  
661 classification processes: General guidelines for practitioners and future research', *Remote Sensing of Environment*, 177, pp. 89–100. Available  
662 at: <https://doi.org/10.1016/j.rse.2016.02.028>.
- 663 Kuhn, M. (2008) 'Building Predictive Models in R Using the caret Package', *Journal of Statistical Software*, 28(5), pp. 1–26. Available at:  
664 <https://doi.org/10.18637/jss.v028.i05>.
- 665 Liddle, D.T. and Elliott, L.P. (2008) 'Tiwi Island threatened plants 2006 to 2008: field survey, population monitoring including establishment of a  
666 program to investigate the impact of pigs, and weed control.', p. 50.

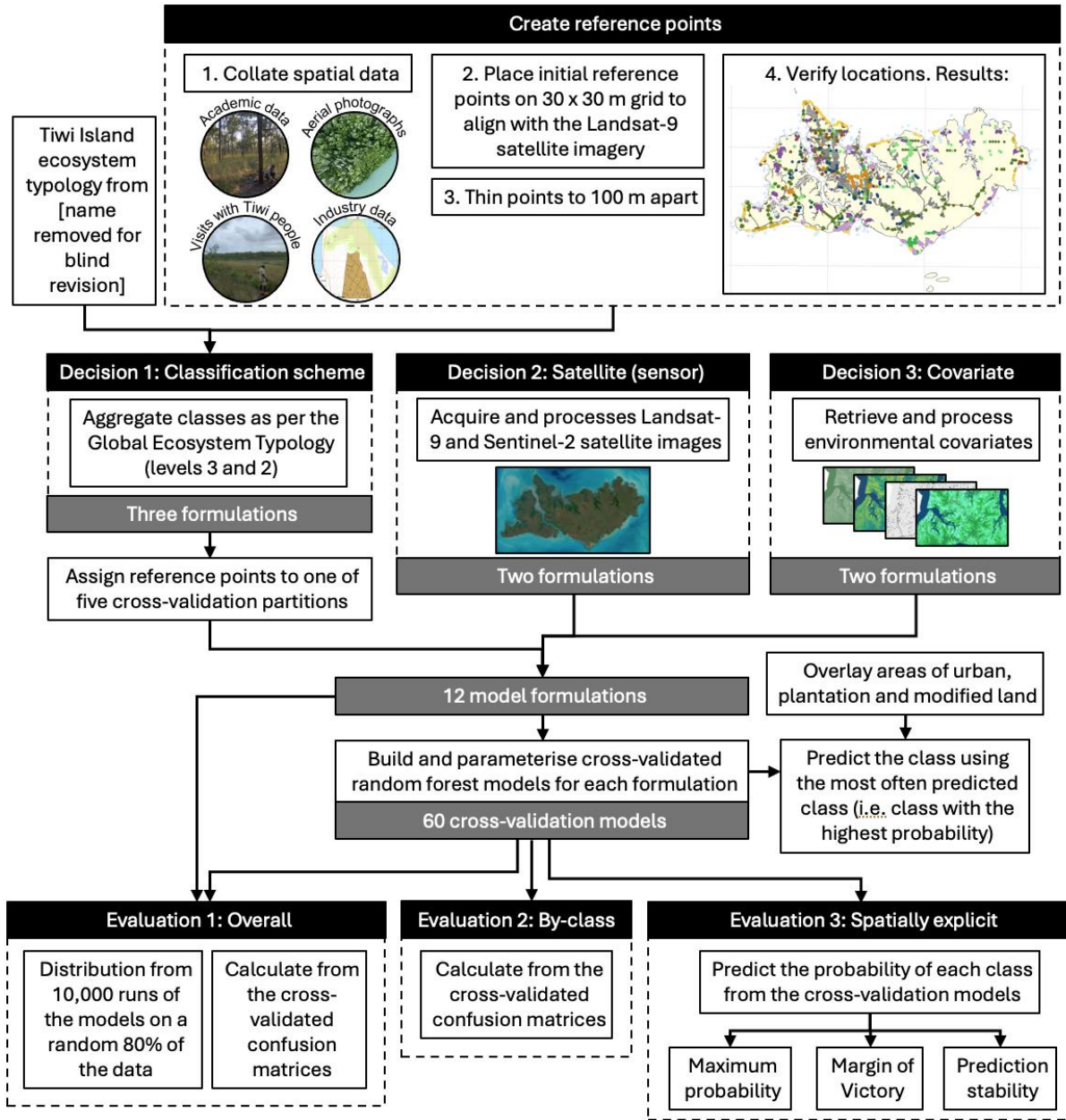
- 667 Loosvelt, L., Peters, J., Skriver, H., Lievens, H., Van Coillie, F.M.B., De Baets, B. and Verhoest, N.E.C. (2012) 'Random Forests as a tool for  
668 estimating uncertainty at pixel-level in SAR image classification', *International Journal of Applied Earth Observation and Geoinformation*, 19, pp.  
669 173–184. Available at: <https://doi.org/10.1016/j.jag.2012.05.011>.
- 670 Maynard, J.J., Yeboah, E., Owusu, S., Buenemann, M., Neff, J.C. and Herrick, J.E. (2023) 'Accuracy of regional-to-global soil maps for on-farm  
671 decision-making: are soil maps "good enough"?' *SOIL*, 9(1), pp. 277–300. Available at: <https://doi.org/10.5194/soil-9-277-2023>.
- 672 McIver, D.K. and Friedl, M.A. (2001) 'Estimating pixel-scale land cover classification confidence using nonparametric machine learning methods',  
673 *IEEE Transactions on Geoscience and Remote Sensing*, 39(9), pp. 1959–1968. Available at: <https://doi.org/10.1109/36.951086>.
- 674 Menkhorst, K.A. and Woinarski, J.C.Z. (1992) 'Distribution of mammals in monsoon rainforests of the Northern Territory', *Wildlife Research*, 19,  
675 pp. 295–316. Available at: <https://doi.org/10.1071/WR9920295>.
- 676 Mitchell, P.J., Downie, A.-L. and Diesing, M. (2018) 'How good is my map? A tool for semi-automated thematic mapping and spatially explicit  
677 confidence assessment', *Environmental Modelling & Software*, 108, pp. 111–122. Available at: <https://doi.org/10.1016/j.envsoft.2018.07.014>.
- 678 Morales-Barquero, L., Lyons, M.B., Phinn, S.R. and Roelfsema, C.M. (2019) 'Trends in Remote Sensing Accuracy Assessment Approaches in the  
679 Context of Natural Resources', *Remote Sensing*, 11(19), p. 2305. Available at: <https://doi.org/10.3390/rs11192305>.
- 680 Mucina, L. (2019) 'Biome: evolution of a crucial ecological and biogeographical concept', *New Phytologist*, 222(1), pp. 97–114. Available at:  
681 <https://doi.org/10.1111/nph.15609>.
- 682 Murray, N.J., Keith, D.A., Bland, L.M., Nicholson, E., Regan, T.J., Rodríguez, J.P. and Bedward, M. (2017) 'The use of range size to assess risks to  
683 biodiversity from stochastic threats', *Diversity and Distributions*, 23(5), pp. 474–483. Available at: <https://doi.org/10.1111/ddi.12533>.
- 684 Murray, N.J., Keith, D.A., Duncan, A., Tizard, R., Ferrer-Paris, J.R., Worthington, T.A., Armstrong, K., Nyan Hlaing, Win Thuya Htut, Aung Htat Oo,  
685 Kyaw Zay Ya and Grantham, H. (2020) 'Myanmar's terrestrial ecosystems: Status, threats and conservation opportunities', *Biological  
686 Conservation*, 252, p. 108834. Available at: <https://doi.org/10.1016/j.biocon.2020.108834>.
- 687 Murray, N.J., Phinn, S.R., DeWitt, M., Ferrari, R., Johnston, R., Lyons, M.B., Clinton, N., Thau, D. and Fuller, R.A. (2019) 'The global distribution  
688 and trajectory of tidal flats', *Nature*, 565(7738), pp. 222–225. Available at: <https://doi.org/10.1038/s41586-018-0805-8>.
- 689 Naas, A.E., Halvorsen, R., Horvath, P., Wollan, A.K., Bratli, H., Brynildsrud, K., Finne, E.A., Keetz, L.T., Lieungh, E., Olson, C., Simensen, T.,  
690 Skarpaas, O., Tandstad, H.R., Torma, M., Værland, E.S. and Bryn, A. (2023) 'What explains inconsistencies in field-based ecosystem mapping?',  
691 *Applied Vegetation Science*, 26(1), p. e12715. Available at: <https://doi.org/10.1111/avsc.12715>.
- 692 Naas, A.E., Keetz, L.T., Halvorsen, R., Horvath, P., Mienna, I.M., Simensen, T. and Bryn, A. (2024) 'Choice of predictors and complexity for  
693 ecosystem distribution models: effects on performance and transferability', *Ecography*, n/a(n/a), p. e07269. Available at:  
694 <https://doi.org/10.1111/ecog.07269>.
- 695 Nagendra, H. and Rocchini, D. (2008) 'High resolution satellite imagery for tropical biodiversity studies: the devil is in the detail', *Biodiversity  
696 and Conservation*, 17(14), pp. 3431–3442. Available at: <https://doi.org/10.1007/s10531-008-9479-0>.
- 697 Neave, G., Murphy, B.P., Tiwi Rangers, Andersen, A. and Davies, H.F. (2024) 'The intact and the imperilled: contrasting mammal population  
698 trajectories between two large adjacent islands', *Wildlife Research* [Preprint].
- 699 Nicholson, E., Andrade, A., Brooks, T.M., Driver, A., Ferrer-Paris, J.R., Grantham, H.S., Gudka, M.S., Keith, D.A., Kontula, T., Lindgaard, A.,  
700 Londono-Murcia, M.C., Murray, N.J., Raunio, A., Rowland, J.A., Sievers, M., Skowno, A.L., Stevenson, S.L., Valderrabano, M., Vernon, C.M.,  
701 Zager, I. and Obura, D. (2024) 'Roles of the Red List of Ecosystems in the Kunming-Montreal Global Biodiversity Framework', *Nature Ecology &  
702 Evolution* [Preprint]. Available at: <https://doi.org/10.1038/s41559-023-02320-5>.
- 703 Noh, J.K., Echeverria, C., Kleemann, J., Koo, H., Fürst, C. and Cuenca, P. (2020) 'Warning about conservation status of forest ecosystems in  
704 tropical Andes: National assessment based on IUCN criteria', *PLOS ONE*. Edited by R. Nóbrega, 15(8), p. e0237877. Available at:  
705 <https://doi.org/10.1371/journal.pone.0237877>.
- 706 Olofsson, P., Arévalo, P., Espejo, A.B., Green, C., Lindquist, E., McRoberts, R.E. and Sanz, M.J. (2020) 'Mitigating the effects of omission errors on  
707 area and area change estimates', *Remote Sensing of Environment*, 236, p. 111492. Available at: <https://doi.org/10.1016/j.rse.2019.111492>.
- 708 Olson, D.M., Dinerstein, E., Wikramanayake, E.D., Burgess, N.D., Powell, G.V.N., Underwood, E.C., D'Amico, J.A., Itoua, I., Strand, H.E., Morrison,  
709 J.C., Loucks, C.J., Allnutt, T.F., Ricketts, T.H., Kura, Y., Lamoreux, J.F., Wettengel, W.W., Hedao, P. and Kassem, K.R. (2001) 'Terrestrial Ecoregions  
710 of the World: A New Map of Life on Earth: A new global map of terrestrial ecoregions provides an innovative tool for conserving biodiversity',  
711 *BioScience*, 51(11), pp. 933–938. Available at: [https://doi.org/10.1641/0006-3568\(2001\)051\[0933:TEOTWA\]2.0.CO;2](https://doi.org/10.1641/0006-3568(2001)051[0933:TEOTWA]2.0.CO;2).

- 712 Pettorelli, N., Laurance, W.F., O'Brien, T.G., Wegmann, M., Nagendra, H. and Turner, W. (2014) 'Satellite remote sensing for applied ecologists:  
713 opportunities and challenges', *Journal of Applied Ecology*. Edited by E.J. Milner-Gulland, 51(4), pp. 839–848. Available at:  
714 <https://doi.org/10.1111/1365-2664.12261>.
- 715 Pettorelli, N., Williams, J., Schulte to Bühne, H. and Crowson, M. (2024) 'Deep learning and satellite remote sensing for biodiversity monitoring  
716 and conservation', *Remote Sensing in Ecology and Conservation* [Preprint]. Available at: <https://doi.org/10.1002/rse2.415>.
- 717 Pontius Jr, R.G. and Millones, M. (2011) 'Death to Kappa: birth of quantity disagreement and allocation disagreement for accuracy assessment',  
718 *International Journal of Remote Sensing*, 32(15), pp. 4407–4429. Available at: <https://doi.org/10.1080/01431161.2011.552923>.
- 719 QGIS Development Team (2018) 'QGIS Geographic Information System'.
- 720 R Core Team (2018) 'R: A language and environment for statistical computing'. Vienna, Austria: R Foundation for Statistical Computing.
- 721 Regan, H.M., Colyvan, M. and Burgman, M.A. (2002) 'A taxonomy and treatment of uncertainty for ecology and conservation biology',  
722 *Ecological Applications*, 12(2), pp. 618–628. Available at: [https://doi.org/10.1890/1051-0761\(2002\)012\[0618:ATATOU\]2.0.CO;2](https://doi.org/10.1890/1051-0761(2002)012[0618:ATATOU]2.0.CO;2).
- 723 Remmel, T.K. (2009) 'Investigating Global and Local Categorical Map Configuration Comparisons Based on Coincidence Matrices', *Geographical  
724 Analysis*, 41(2), pp. 144–157. Available at: <https://doi.org/10.1111/j.1538-4632.2009.00738.x>.
- 725 Richards, A.E., Andersen, A.N., Schatz, J., Eager, R., Dawes, T.Z., Hadden, K., Scheepers, K. and Van Der Geest, M. (2012) 'Savanna burning,  
726 greenhouse gas emissions and indigenous livelihoods: Introducing the Tiwi Carbon Study: THE TIWI CARBON STUDY', *Austral Ecology*, 37(6), pp.  
727 712–723. Available at: <https://doi.org/10.1111/j.1442-9993.2012.02395.x>.
- 728 Rivas, C.A., Guerrero-Casado, J. and Navarro-Cerillo, R.M. (2021) 'Deforestation and fragmentation trends of seasonal dry tropical forest in  
729 Ecuador: impact on conservation', *Forest Ecosystems*, 8(1), p. 46. Available at: <https://doi.org/10.1186/s40663-021-00329-5>.
- 730 Rocchini, D., Foody, G.M., Nagendra, H., Ricotta, C., Anand, M., He, K.S., Amici, V., Kleinschmit, B., Förster, M., Schmidlein, S., Feilhauer, H.,  
731 Ghisla, A., Metz, M. and Neteler, M. (2013) 'Uncertainty in ecosystem mapping by remote sensing', *Computers & Geosciences*, 50, pp. 128–135.  
732 Available at: <https://doi.org/10.1016/j.cageo.2012.05.022>.
- 733 Rossiter, D.G., Poggio, L., Beaudette, D. and Libohova, Z. (2022) 'How well does digital soil mapping represent soil geography? An investigation  
734 from the USA', *SOIL*, 8(2), pp. 559–586. Available at: <https://doi.org/10.5194/soil-8-559-2022>.
- 735 RStudio Team (2020) 'RStudio: Integrated Development for R'. Boston, MA: RStudio, PBC. Available at: <http://www.rstudio.com>.
- 736 Russell-Smith, J. (1991) 'Classification, species richness, and environmental relations of monsoon rain forest in northern Australia', *Journal of  
737 Vegetation Science*, 2(2), pp. 259–278. Available at: <https://doi.org/10.2307/3235959>.
- 738 Scarth, P., Armston, J., Lucas, R. and Bunting, P. (2023) 'Vegetation Height and Structure - Derived from ALOS-1 PALSAR, Landsat and  
739 ICESat/GLAS, Australia Coverage.' Available at: <https://portal.tern.org.au/metadata/TERN/de1c2fef-b129-485e-9042-8b22ee616e66>.
- 740 Simensen, T., Horvath, P., Vollering, J., Erikstad, L., Halvorsen, R. and Bryn, A. (2020) 'Composite landscape predictors improve distribution  
741 models of ecosystem types', *Diversity and Distributions*, 26(8), pp. 928–943. Available at: <https://doi.org/10.1111/ddi.13060>.
- 742 Smith, A., Murphy, S., Herderson, D. and Erickson, K. (2023) 'Including imprecisely georeferenced specimens improves accuracy of species  
743 distribution models and estimates of niche breadth', *Global Ecology & Biogeography*, 32(3), pp. 342–355. Available at:  
744 <https://doi.org/doi:10.1111/geb.13628>.
- 745 Stehman, S.V. (2009) 'Sampling designs for accuracy assessment of land cover', *International Journal of Remote Sensing*, 30(20), pp. 5243–5272.  
746 Available at: <https://doi.org/10.1080/01431160903131000>.
- 747 Stehman, S.V. and Foody, G.M. (2019) 'Key issues in rigorous accuracy assessment of land cover products', *Remote Sensing of Environment*,  
748 231, p. 111199. Available at: <https://doi.org/10.1016/j.rse.2019.05.018>.
- 749 Trouvé, R., Jiang, R., Fedrigo, M., White, M.D., Kasel, S., Baker, P.J. and Nitschke, C.R. (2023) 'Combining Environmental, Multispectral, and  
750 LiDAR Data Improves Forest Type Classification: A Case Study on Mapping Cool Temperate Rainforests and Mixed Forests', *Remote Sensing*,  
751 15(1), p. 60. Available at: <https://doi.org/10.3390/rs15010060>.
- 752 UNSD (2021) *System of Environmental-Economic Accounting—Ecosystem Accounting: Final Draft version 5*. Department of Economic and Social  
753 Affairs, Statistical Division, United Nations, pp. 1–350. Available at: [https://unstats.un.org/unsd/envaccounting/seeaRev/SEEA\\_CF\\_Final\\_en.pdf](https://unstats.un.org/unsd/envaccounting/seeaRev/SEEA_CF_Final_en.pdf)  
754 (Accessed: 24 January 2024).

- 755 Venter, Z.S., Barton, D.N., Chakraborty, T., Simensen, T. and Singh, G. (2022) 'Global 10 m Land Use Land Cover Datasets: A Comparison of  
756 Dynamic World, World Cover and Esri Land Cover', *Remote Sensing*, 14(16), p. 4101. Available at: <https://doi.org/10.3390/rs14164101>.
- 757 Venter, Z.S., Czúcz, B., Stange, E., Nowell, M.S., Simensen, T., Immerzeel, B. and Barton, D.N. (2024) "'Uncertainty audit" for ecosystem  
758 accounting: Satellite-based ecosystem extent is biased without design-based area estimation and accuracy assessment', *Ecosystem Services*, 66,  
759 p. 101599. Available at: <https://doi.org/10.1016/j.ecoser.2024.101599>.
- 760 Viscarra Rossel, R.A., Chen, C., Grundy, M.J., Searle, R., Clifford, D. and Campbell, P.H. (2015) 'The Australian three-dimensional soil grid:  
761 Australia's contribution to the GlobalSoilMap project', *Soil Research*, 53(8), p. 845. Available at: <https://doi.org/10.1071/SR14366>.
- 762 Watson, J.E.M., Keith, D.A., Strassburg, B.B.N., Venter, O., Williams, B. and Nicholson, E. (2020) 'Set a global target for ecosystems', *Nature*,  
763 578(7795), pp. 360–362. Available at: <https://doi.org/10.1038/d41586-020-00446-1>.
- 764 Watson, J.E.M., Venegas-Li, R., Grantham, H., Dudley, N., Stolton, S., Rao, M., Woodley, S., Hockings, M., Burkart, K., Simmonds, J.S., Sonter, L.J.,  
765 Sreekar, R., Possingham, H.P. and Ward, M. (2023) 'Priorities for protected area expansion so nations can meet their Kunming-Montreal Global  
766 Biodiversity Framework commitments', *Integrative Conservation*, 2(3), pp. 140–155. Available at: <https://doi.org/10.1002/inc3.24>.
- 767 Whittaker, R.H. (1956) 'Vegetation of the Great Smoky Mountains', *Ecological Monographs*, 26(1), pp. 2–80. Available at:  
768 <https://doi.org/10.2307/1943577>.
- 769 Wilson, B.A. and Fensham, R.J. (1994) 'A comparison of classification systems for the conservation of sparsely wooded plains on Melville Island,  
770 Northern Australia', *Australian Geographer*, 25(1), pp. 18–31. Available at: <https://doi.org/10.1080/00049189408703095>.
- 771 Wohlfart, C., Wegmann, M. and Leimgruber, P. (2014) 'Mapping Threatened Dry Deciduous Dipterocarp Forest in South-East Asia for  
772 Conservation Management', *Tropical Conservation Science*, 7(4), pp. 597–613. Available at: <https://doi.org/10.1177/194008291400700402>.
- 773 Wright, M.N. and Ziegler, A. (2017) 'Ranger: a fast implementation of random forests for high dimensional data in C++ and R.', *Journal of*  
774 *Statistical Software*, 77(1), pp. 1–17. Available at: <https://doi.org/doi:10.18637/jss.v077.i01>.
- 775 Wulder, M.A., Masek, J.G., Cohen, W.B., Loveland, T.R. and Woodcock, C.E. (2012) 'Opening the archive: How free data has enabled the science  
776 and monitoring promise of Landsat', *Remote Sensing of Environment*, 122, pp. 2–10. Available at: <https://doi.org/10.1016/j.rse.2012.01.010>.
- 777 Xiao, H., Driver, A., Etter, A., Keith, D.A., Obst, C., Traurig, M.J. and Nicholson, E. (2024) 'Synergies and complementarities between ecosystem  
778 accounting and the Red List of Ecosystems', *Nature Ecology & Evolution*, 8, pp. 1794–1803. Available at: <https://doi.org/10.1038/s41559-024-02494-6>.
- 780 Young, A.R., Davies, H.F., Ayre, M.L., Brekelmans, A., Bryan, B.A., Elith, J., Hadden, K., Kerinaia, M., Keith, D.A., Lewis, D.L., Munkara-Murray,  
781 K.M., Ryan, S., Spencer, M. and Nicholson, E. (2024) 'Applying the Global Ecosystem Typology to classify, describe, and map ecosystems from  
782 regional data and Indigenous knowledge'. EcoEvoRxiv. Available at: <https://doi.org/10.32942/X20P75>.
- 783 Yu, Le, Liang, L., Wang, J., Zhao, Y., Cheng, Q., Hu, L., Liu, S., Yu, Liang, Wang, X., Zhu, P., Li, Xueyan, Xu, Y., Li, C., Fu, W., Li, Xuecao, Li, W., Liu, C.,  
784 Cong, N., Zhang, H., Sun, F., Bi, X., Xin, Q., Li, D., Yan, D., Zhu, Z., Goodchild, M.F. and Gong, P. (2014) 'Meta-discoveries from a synthesis of  
785 satellite-based land-cover mapping research', *International Journal of Remote Sensing*, 35(13), pp. 4573–4588. Available at:  
786 <https://doi.org/10.1080/01431161.2014.930206>.

787 **Appendix**

788 **Appendix S1 – Modelling methodology overview**



789

790 Figure S1.5 Flow chart of the methods to test three modelling decisions on mapping the extent

791 of ecosystems and assess the decisions with three assessment metrics.

792 **Appendix S2 – Software**

793 **Software**

794 QGIS (version 3.22.12)

795 Google Earth Engine (Gorelick et al., 2017)

796 R (version 4.3.0) (R Core Team, 2018)

797 R-studio (version 2023.09.1+949) (RStudio Team, 2020)

798

799 **R packages**

800 Satellite imagery and environmental covariates:

801 'rgee' (version 1.1.6.9999) (Aybar *et al.*, 2020)

802 'rgeeExtra' (version 0.0.1) (Aybar *et al.*, 2020)

803 Data cleaning and manipulation:

804 'enmSdmX' package (version 1.1.2) (Smith *et al.*, 2023)

805 'dplyr' (version 1.1.2) (Wickham *et al.*, 2023)

806 'tidyr' (version 1.3.0) (Wickham, Vaughan and Girlich, 2023)

807 'stringr' (version 1.5.0) (Wickham, 2022)

808 Spatial data handling:

809 'sf' (version 1.0-16) (Pebesma, 2018)

810 'terra' (version 1.7-29) (Hijmans, 2023)

811 Model fitting, evaluation and prediction:

812 'ranger' (version 0.15.1) (Wright and Ziegler, 2017)

813 'vip' (version 0.3.2) (Greenwell and Boehmke, 2020)

814 'caret' (version 6.0-94) (Kuhn, 2008)  
815 Visualisations:  
816 'tidytterra' (version 0.4.0) (Hernangomez, 2024)  
817 'ggplot2' (version 3.4.3) (Wickham, 2016)  
818 'ggspatial' (version 1.1.8) (Dunnington, 2023)  
819 'ggh4x' (version 0.2.8) (van den Brand, 2024)  
820 'ggnewscale' (version 0.4.9) (Campitelli, 2023)  
821 'ggstance' (version 0.3.7) (Henry, Wickham and Chang, 2024)

## 822 **Appendix S3 – Satellite imager processing**

823 We applied scaling factors to the satellite images obtained from the Landsat-9 satellite with the  
824 OLI-2 sensor and from the Sentinel-2 satellite with the MSI sensor. For the optical bands (i.e.  
825 the name begins with SR) of Landsat-9 OLI images, the band was first multiplied by  $2.75 \times 10^{-5}$   
826 then minus 0.2. For the thermal bands (i.e. the name begins with ST) of Landsat-9, the band  
827 was first multiplied by  $3.41802 \times 10^{-3}$  then added 149. The Sentinel-2 images were scaled by  
828 0.0001 to reverse the scaling factor applied for efficient data storage.

829  
830 To mask the clouds in the Landsat-9 images, we used the quality assessment bands for the  
831 cloud and cloud shadow (bits 3 and 5). For the Sentinel-2 images, we used the Scene  
832 Classification Layer and removed the pixels classified as no data (SCL = 0), saturated (SCL = 1),  
833 medium or high cloud probability (SCL = 8 and 9), high cirrus cloud (SCL = 10), snow and ice (SCL  
834 = 11).

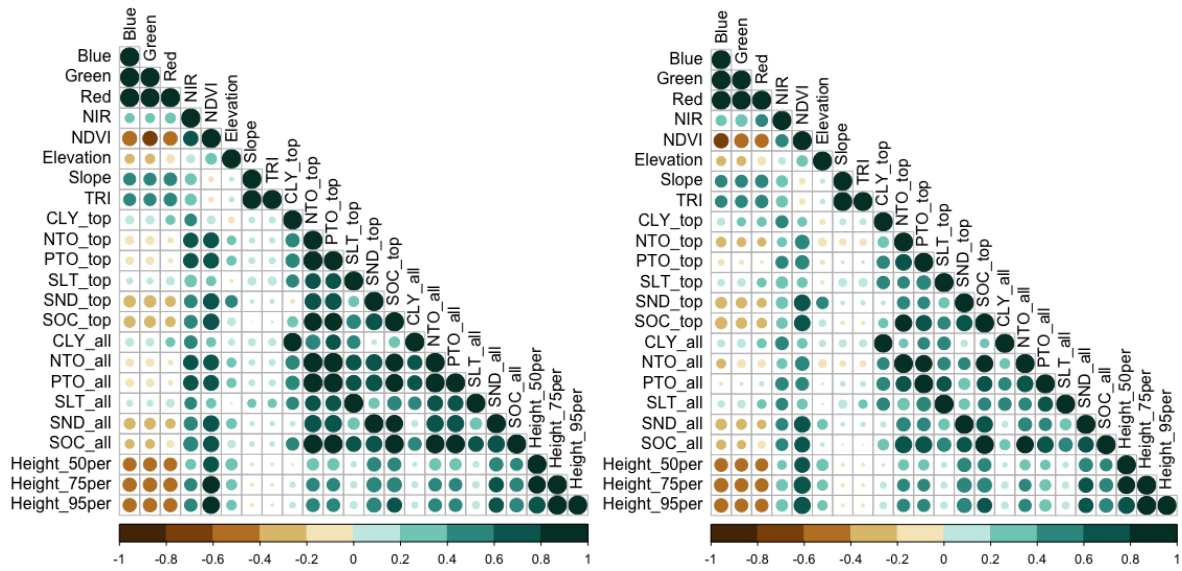
835 **Appendix S4 – Environmental covariates**

836 We tested correlation in the variables using the absolute value of the Pearson’s correlation  
837 coefficient with a cut-off of 0.7 (Figure 2). The red, green and blue bands were all highly  
838 correlated. NDVI was least correlated to the red band for both satellites.

839 Each of the soil variables were correlated between the two depths. We retained the top 30 cm  
840 variables to reflect the root zone of more of the plant species. Nitrogen, phosphorus and soil  
841 sand content were highly correlated to near infrared and NDVI for the Landsat-9 variables and  
842 hence removed. We retained slope instead of the correlated TRI to represent rainfall run-off  
843 and easier interpretation of the results. Each of the vegetation biomass height variables were  
844 correlated. We retained the height of 50% of the biomass as it was least correlated to all the  
845 other covariates.

846 Table S4.2. Details of the environmental covariates.

Layer	Description	Rational	Source
<i>Satellite image covariates</i>			
Red Green Blue NIR	The red, green, blue and near infrared bands.	Spectral characteristics represent physical and chemical attributes of the ecosystem.	Landsat-9 satellite atmospherically corrected surface reflectance (level 2, collection 2, tier 1) courtesy of the United States Geological Survey (USGS). For Landsat-9, the red band is B4, green is B3, blue is B2 and near infrared is B5. Sentinel-2 surface reflectance harmonised collection (level-2A) with atmospheric correction from the Copernicus Sentinel missions are by the European Space Agency (ESA). For Sentinel-2, the red band is B4, green is B3, blue is B2 and near infrared is B8.
NDVI	Normalised difference vegetation index.	Greenness of the canopy which is correlated to primary productivity.	Calculated from the satellite image using the red and near infrared bands where: $\text{NDVI} = \frac{\text{NIR} - \text{Red}}{\text{NIR} + \text{Red}}$
<i>Additional covariates</i>			
Height_50 Height_75 Height_95	The height where 50, 75 and 95% of the plant cover has been intercepted.	The height of the vegetation biomass relates to the vegetation structure.	Terrestrial Ecosystem Research Network <a href="https://portal.tern.org.au/metadatas/TERN/de1c2fef-b129-485e-9042-8b22ee616e66">https://portal.tern.org.au/metadatas/TERN/de1c2fef-b129-485e-9042-8b22ee616e66</a>
Elev	Elevation in meters.	The elevation is a proxy for range of environmental relationships including access to groundwater, influence of floods, exposure to wind on hilltops, and exposure to wave disturbances on coastal ecosystem. The topographic measures of the slope, position and roughness also relate to soil moisture and run off which strongly drive ecosystem functioning.	The Smoothed Digital Elevation model (DEM-S) at a 5 m resolution from the Shuttle Radar Topography Mission (SRTM) by from Geoscience Australia in 2000 <a href="https://developers.google.com/earth-engine/datasets/catalog/AU_GA_DEM_1SEC_v10_DEM-S">https://developers.google.com/earth-engine/datasets/catalog/AU_GA_DEM_1SEC_v10_DEM-S</a>
Slp	Slope in degrees.		Created using the 'terrain' function from the 'terra' package in R on the elevation model. Slope was computed with the four neighbouring cells and measured in degrees.
TRI	Topographic roughness index.		
Clay Silt Sand SOC NTO PTO	Percentage of 1) clay, 2) silt, 3) sand, 4) soil organic carbon, 5) nitrogen or 6) phosphorus in the top 30 cm and 2 m of the soil.	The soil composition influences many aspects of plant growth and soil moisture, including nutrient availability and drainage.	Soil and Landscape Grid of Australia. Averaged by the depth over which the attribute was measured (depth-weighted average). <a href="https://dx.doi.org/10.1071/SR14366">https://dx.doi.org/10.1071/SR14366</a>



847 Figure S4.6. Correlation of the environmental predictors at a 30 m resolution with Landsat-9  
 848 satellite imagery using the OLI-2 sensor (left) and a 10 m resolution with Sentinel-2 satellite  
 849 imagery using the MSI sensor (right).

850

851 **Appendix S5 – Model evaluation**

852 For the confusion matrix

		Reference	
		1	0
Predicted	1	<i>a</i>	<i>b</i>
	0	<i>c</i>	<i>d</i>

856 *a* represents the number of true positive values, *b* the false positives, *c* the false negatives and

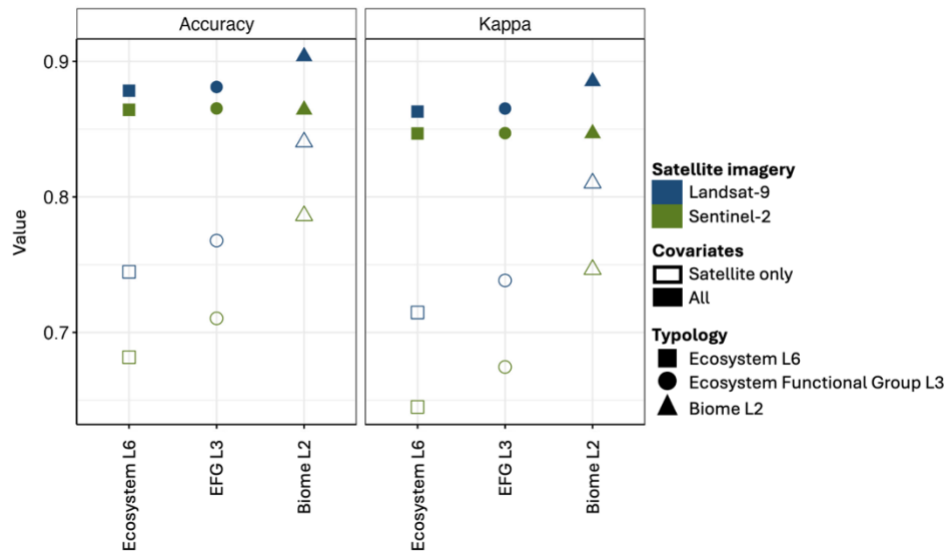
857 *d* the true negatives. This confusion matrix is used to calculate the evaluation metrics in

858 Table S5.3.

859 Table S5.3. Descriptions of the overall and by-class evaluation metrics.

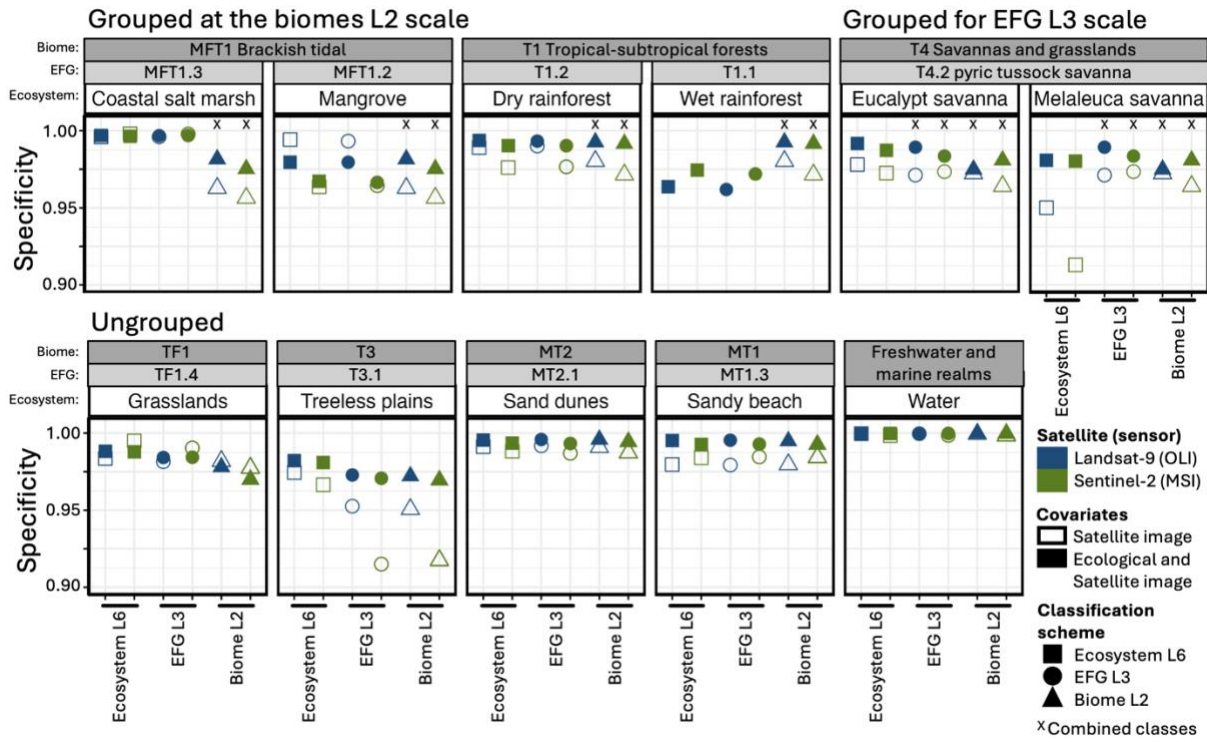
Evaluation metric	Other names	Equation	Description
<i>Overall metrics</i>			
Accuracy		$\frac{a + d}{a + b + c + d}$	A measure of agreement between the predicted and true values, such that 1 indicates perfect agreements and 0 indicates no agreement.
Kappa statistic	Cohen’s kappa	$N = a + b + c + d$ $p_e = \frac{a + c}{N} \times \frac{a + b}{N} + \frac{b + d}{N} \times \frac{c + d}{N}$ $Kappa = \frac{p_0 - p_e}{1 - p_e}$	A measure of agreement between the predicted and true values, such that 1 indicates perfect agreements and 0 indicates no more agreement than expected by chance.
Out-of-bag error (OOB)	Out-of-bag score		The average error for the random forest trees using bootstrap aggregation and calculated on the out-of-bag samples.
<i>By-class metrics</i>			
Sensitivity	Producer’s accuracy, recall, true positive rate	$\frac{a}{a + c}$	The ability of the model to correctly identify all the true cases from those known to be true.
Specificity	True negative rate	$\frac{d}{b + d}$	The ability of the model to correctly identify all the false cases from those known to be false.
Precision	User’s accuracy, positive predicted value	$\frac{a}{a + b}$	The ability of the model to correctly identify all the true cases from those predicted to the class.
F1		$2 \times \frac{Sensitivity \times Precision}{Sensitivity + Precision}$	A balance of the models ability to predict the true cases from thoses known to be true (i.e. sensitivity) and the correctly true from all those predicted to be true (i.e. precision).
Negative predicted value		$\frac{d}{c + d}$	The ability of the model to correctly identify all the false cases from those predicted to be false.

860 **Appendix S6 – Additional model results**

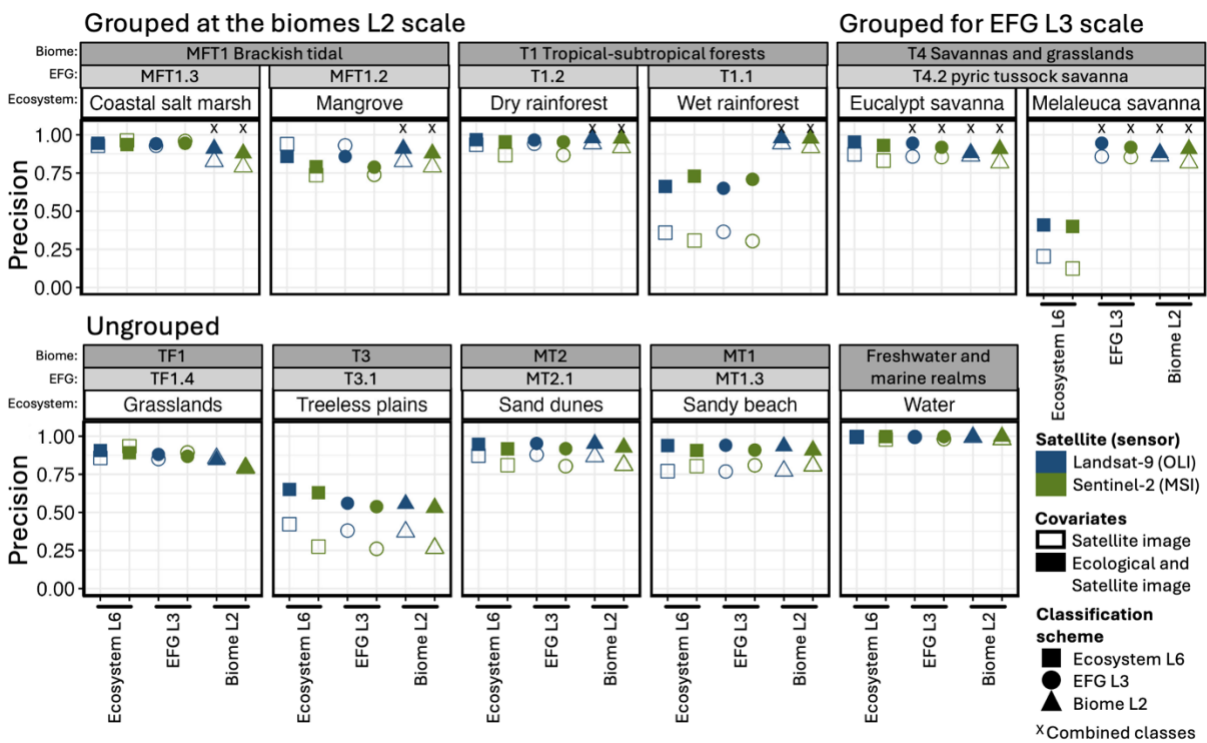


861 Figure S6.7. The mean accuracy and kappa statistics calculated from the confusion matrix of 12  
 862 model formulations varying at three modelling decisions and each run with five cross-validated  
 863 models. The modelling decisions were the typology (shape), covariates (fill) and satellite  
 864 imagery (colours).

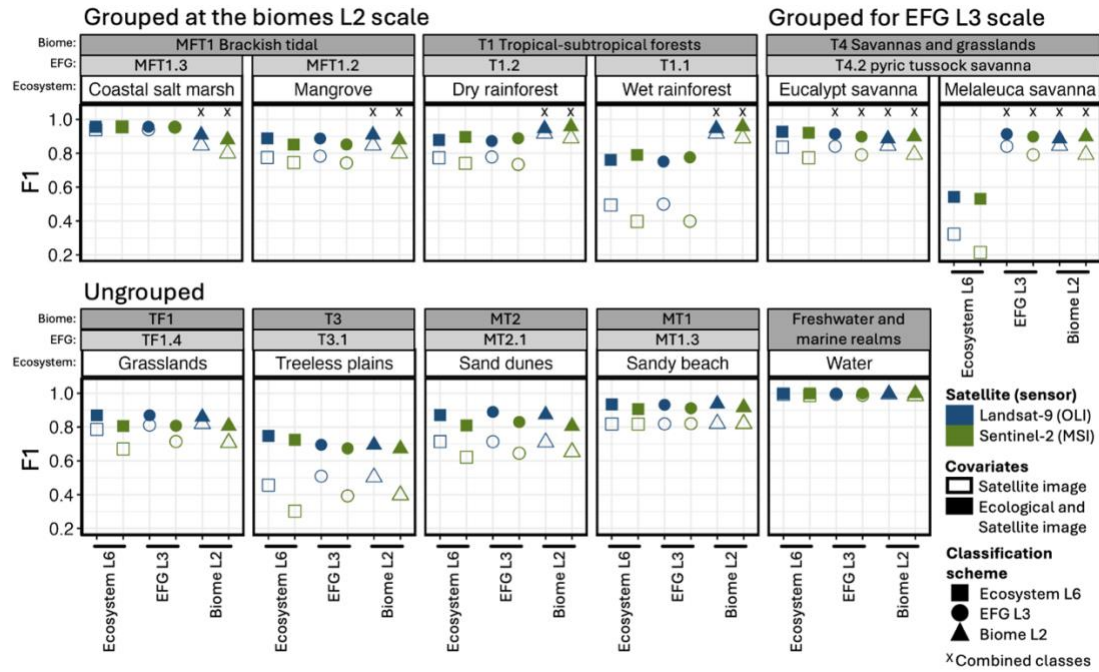
A)



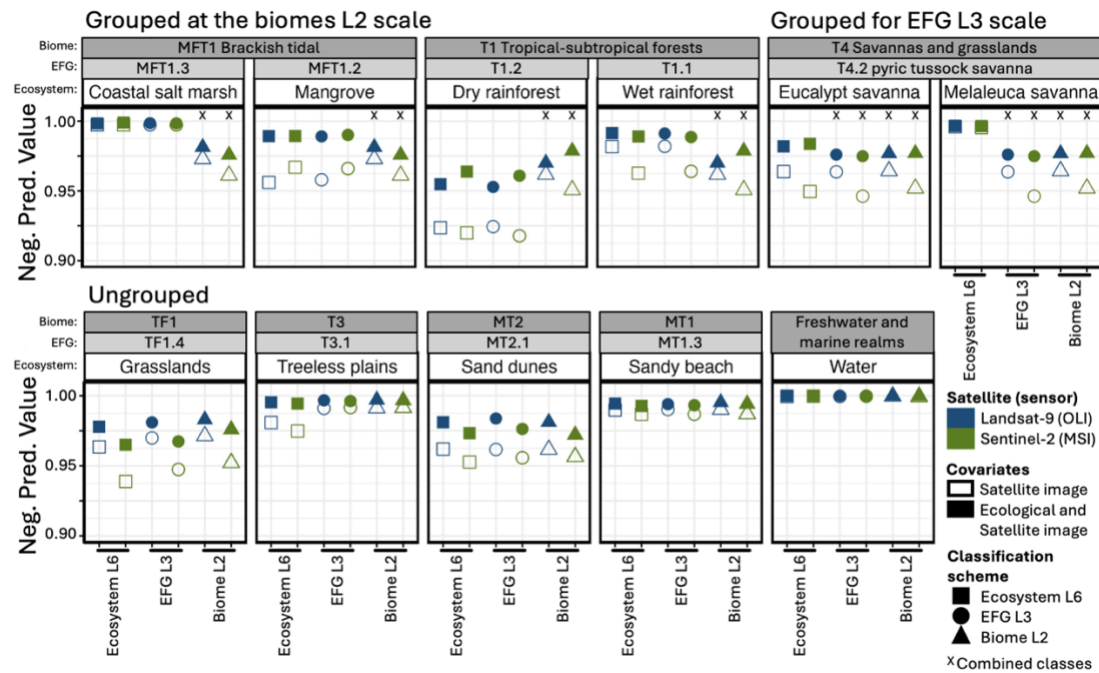
B)



C)

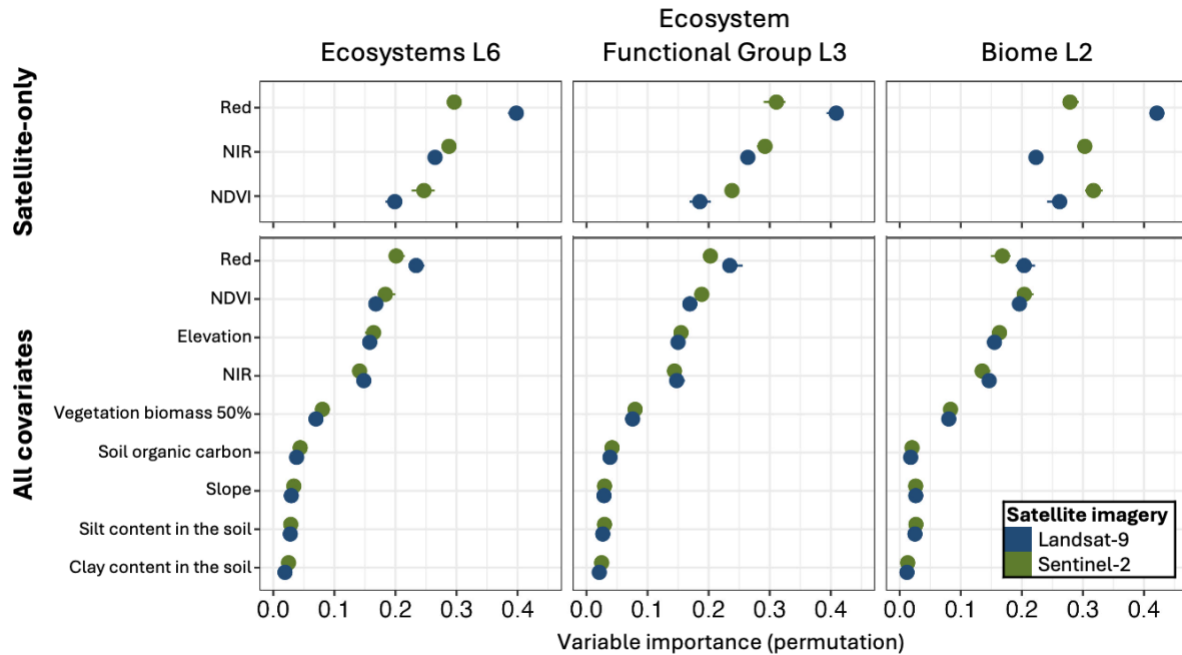


D)



865 Figure S6.8. The four by-class evaluation metrics specificity (A), precision (B), F1 (C), and  
 866 negative predicted value (D) measured for three classification schemes (shape), two  
 867 satellite/sensors (colour) and two covariate sets (fill). When multiple ecosystems (shape:

868 square, label above: white) were aggregated into an ecosystem functional group (shape: circle,  
 869 label: light grey) or into a biome (shape: triangle, label: dark grey), the class is indicated by an x.



870  
 871 Figure S6.9. Importance of the environmental covariates in the ecosystem classification model  
 872 across three classification schemes (columns), two options for the covariates (row) and two  
 873 satellite (colours). NDVI is for the normalised difference vegetation index and NIR is for the  
 874 near-infrared band from the satellite image.

875

876 Table S6.4. Confusion matrix for the ecosystem classification model using Landsat-9 satellite  
 877 imagery from the OLI-2 sensor as the only covariates.

	Training points												UA	CE
	Coastal salt marsh	Dry rainforest	Eucalypt savanna	Grassland and sedgeland	Mangrove	Melaleuca savanna	Treeless plains	Sand dunes	Sandy beach	Water	Wet rainforest	Total		
Coastal salt marsh	285	0	0	4	1	0	0	1	13	3	0	307	0.93	0.07
Dry rainforest	0	754	0	0	2	0	0	0	0	0	50	806	0.94	0.06
Eucalypt savanna	0	7	745	42	9	9	20	14	0	0	8	854	0.87	0.13
Grassland and sedgeland	7	0	13	511	43	1	4	2	0	0	15	596	0.86	0.14
Mangrove	0	3	0	10	461	0	0	0	0	0	17	491	0.94	0.06
Melaleuca savanna	0	1	111	76	0	74	79	22	0	0	0	363	0.20	0.80
Treeless plains	0	1	39	26	0	12	106	67	0	0	0	251	0.42	0.58
Sand dunes	1	0	0	0	0	0	5	321	41	0	0	368	0.87	0.13
Sandy beach	7	0	0	0	0	0	0	104	373	0	0	484	0.77	0.23
Water	0	0	0	1	0	0	0	0	1	411	0	413	1.00	0.00
Wet rainforest	0	376	19	34	182	0	0	0	0	0	343	954	0.36	0.64
Total	300	1142	927	704	698	96	214	531	428	414	433	5887		
PA	0.95	0.66	0.80	0.73	0.66	0.77	0.50	0.60	0.87	0.99	0.79			
OE	0.05	0.34	0.20	0.27	0.34	0.23	0.50	0.40	0.13	0.01	0.21			

Model formulation

**Classification scheme:** Ecosystem (level 6 of the Global Ecosystem typology)

**Satellite/sensor:** Landsat-9/OLI-2

**Covariate set:** Satellite image covariates only

PA: Producer's accuracy

UA: User's accuracy

OE: Omission error

CE: Commission error

878

879 Table S6.5. Confusion matrix for the ecosystem classification model using Landsat-9 satellite  
 880 imagery from the OLI-2 sensor and using satellite image and additional covariates.

	Training points												Total	UA	CE
	Coastal salt marsh	Dry rainforest	Eucalypt savanna	Grassland and sedgeland	Mangrove	Melaleuca savanna	Treeless plains	Sand dunes	Sandy beach	Water	Wet rainforest				
Coastal salt marsh	291	0	0	8	1	0	0	1	7	0	0	308	0.94	0.06	
Dry rainforest	0	919	0	0	6	0	0	0	0	0	24	949	0.97	0.03	
Eucalypt savanna	0	3	83	18	5	1	1	5	0	0	8	878	0.95	0.05	
Grassland and sedgeland	3	0	6	588	36	1	4	5	0	0	6	649	0.91	0.09	
Mangrove	0	45	1	52	64	3	0	0	1	0	7	749	0.86	0.14	
Melaleuca savanna	0	1	37	18	2	77	21	32	0	0	0	188	0.41	0.59	
Treeless plains	0	0	27	19	0	17	18	8	38	0	0	289	0.65	0.35	
Sand dunes	1	1	0	0	0	0	0	42	8	22	0	452	0.95	0.05	
Sandy beach	5	0	0	0	0	0	0	21	39	8	0	424	0.94	0.06	
Water	0	0	0	0	0	0	0	0	1	41	4	415	1.00	0.00	
Wet rainforest	0	173	19	1	5	96	0	0	0	0	38	586	0.66	0.34	
Total	300	1142	927	704	698	964	44	513	428	414	433	5887			
PA	0.97	0.80	0.90	0.84	0.90	0.80	0.80	0.80	0.90	1.00	0.90				
OE	0.03	0.20	0.10	0.16	0.10	0.20	0.20	0.20	0.10	0.00	0.10				

Model formulation

**Classification scheme:** Ecosystem (level 6 of the Global Ecosystem typology)

**Satellite/sensor:** Landsat-9/OLI-2

**Covariate set:** Satellite image and additional covariates

PA: Producer's accuracy

UA: User's accuracy

OE: Omission error

CE: Commission error

881

882 Table S6.6. Confusion matrix for the ecosystem classification model using Sentinel-2 satellite  
 883 imagery from the MSI sensor as the only covariates.

	Training points											Total	UA	CE
	Coastal salt marsh	Dry rainforest	Eucalypt savanna	Grassland and sedgeland	Mangrove	Melaleuca savanna	Treeless plains	Sand dunes	Sandy beach	Water	Wet rainforest			
Coastal salt marsh	285	0	0	3	1	0	0	1	5	1	0	296	0.96	0.04
Dry rainforest	0	739	0	2	17	0	0	1	0	0	93	852	0.87	0.13
Eucalypt savanna	0	2	671	45	16	16	23	12	0	0	22	807	0.83	0.17
Grassland and sedgeland	3	0	1	368	11	3	3	3	0	0	2	394	0.93	0.07
Mangrove	0	55	0	61	527	0	0	1	0	0	72	716	0.74	0.26
Melaleuca savanna	0	0	217	137	3	72	113	33	0	0	1	576	0.13	0.88
Treeless plains	0	0	19	31	0	5	72	131	4	0	0	262	0.27	0.73
Sand dunes	2	0	0	0	0	0	3	268	58	0	0	331	0.81	0.19
Sandy beach	7	0	0	0	0	0	0	79	356	1	0	443	0.80	0.20
Water	3	0	0	1	0	0	0	0	5	412	0	421	0.98	0.02
Wet rainforest	0	346	19	56	123	0	0	2	0	0	243	789	0.31	0.69
Total	300	1142	927	704	698	96	214	531	428	414	433	5887		
PA	0.95	0.65	0.72	0.52	0.76	0.75	0.34	0.5	0.83	1.00	0.56			
OE	0.05	0.35	0.28	0.48	0.24	0.25	0.66	0.5	0.17	0.00	0.44			

Model formulation

**Classification scheme:** Ecosystem (level 6 of the Global Ecosystem typology)

**Satellite/sensor:** Sentinel-2/MSI

**Covariate set:** Satellite image covariates only

PA: Producer's accuracy

UA: User's accuracy

OE: Omission error

CE: Commission error

884

885 Table S6.7 . Confusion matrix for the ecosystem classification model using Sentinel-2 satellite  
 886 imagery from the MSI sensor and using satellite image and additional covariates.

	Training points												Total	UA	CE
	Coastal salt marsh	Dry rainforest	Eucalypt savanna	Grassland and sedgeland	Mangrove	Melaleuca savanna	Treeless plains	Sand dunes	Sandy beach	Water	Wet rainforest				
Coastal salt marsh	294	0	0	7	1	0	0	5	7	0	0	314	0.94	0.06	
Dry rainforest	0	966	1	1	16	0	0	1	0	0	27	1012	0.95	0.05	
Eucalypt savanna	0	1	846	30	5	0	2	4	0	0	21	909	0.93	0.07	
Grassland and sedgeland	1	1	4	518	26	3	6	19	1	0	2	581	0.89	0.11	
Mangrove	0	51	1	107	644	0	0	3	0	0	8	814	0.79	0.21	
Melaleuca savanna	0	0	34	21	2	76	21	35	0	0	1	190	0.40	0.60	
Treeless plains	0	0	30	17	0	16	183	44	1	0	0	291	0.63	0.37	
Sand dunes	0	0	1	2	0	0	2	385	30	0	0	420	0.92	0.08	
Sandy beach	5	0	0	0	0	0	0	35	388	0	0	428	0.91	0.09	
Water	0	0	0	0	0	0	0	0	1	414	0	415	1.00	0.00	
Wet rainforest	0	123	10	1	4	1	0	0	0	0	374	513	0.73	0.27	
<b>Total</b>	<b>300</b>	<b>1142</b>	<b>927</b>	<b>704</b>	<b>698</b>	<b>96</b>	<b>214</b>	<b>531</b>	<b>428</b>	<b>414</b>	<b>433</b>	<b>5887</b>			
PA	0.98	0.85	0.91	0.74	0.92	0.79	0.86	0.73	0.91	1.00	0.86				
OE	0.02	0.15	0.09	0.26	0.08	0.21	0.14	0.27	0.09	0.00	0.14				

Model formulation

**Classification scheme:** Ecosystem (level 6 of the Global Ecosystem typology)

**Satellite/sensor:** Sentinel-2/MSI

**Covariate set:** Satellite image and additional covariates

PA: Producer's accuracy

UA: User's accuracy

OE: Omission error

CE: Commission error

887

888 Table S6.8. Confusion matrix for the ecosystem functional group classification model using  
 889 Landsat-9 satellite imagery from the OLI-2 sensor as the only covariates.

	Training points											Total	UA	CE
	Dry rainforest	Grassland and sedgeland	Mangrove	Coastal salt marsh	Sandy beach	Sand dunes	Savanna	Treeless plains	Water	Wet rainforest				
Dry rainforest	758	0	2	0	0	0	0	0	0	45	805	0.94	0.06	
Grassland and sedgeland	1	546	41	7	0	6	22	5	0	14	642	0.85	0.15	
Mangrove	3	10	472	0	0	0	0	0	0	22	507	0.93	0.07	
Coastal salt marsh	0	4	1	285	13	1	0	0	3	0	307	0.93	0.07	
Sandy beach	0	0	0	7	375	106	0	0	0	0	488	0.77	0.23	
Sand dunes	0	0	0	1	39	319	0	4	0	0	363	0.88	0.12	
Savanna	7	60	9	0	0	16	845	40	0	8	985	0.86	0.14	
Treeless plains	0	49	0	0	0	83	137	165	0	0	434	0.38	0.62	
Water	0	1	0	0	1	0	0	0	411	0	413	1.00	0.00	
Wet rainforest	373	34	173	0	0	0	19	0	0	344	943	0.36	0.64	
Total	1142	704	698	300	428	531	1023	214	414	433	5887			
PA	0.66	0.78	0.68	0.95	0.88	0.60	0.83	0.77	0.99	0.79				
OE	0.34	0.22	0.32	0.05	0.12	0.40	0.17	0.23	0.01	0.21				

Model formulation

**Classification scheme:** Ecosystem Functional Group (level 3 of the Global Ecosystem typology)

**Satellite/sensor:** Landsat-9/OLI-2

**Covariate set:** Satellite image covariates only

PA: Producer's accuracy

UA: User's accuracy

OE: Omission error

CE: Commission error

890

891 Table S6.9. Confusion matrix for the ecosystem functional group classification model using  
 892 Landsat-9 satellite imagery from the OLI-2 sensor and using the satellite image and additional  
 893 covariates.

	Training points											UA	CE
	Dry rainforest	Grassland and sedgeland	Mangrove	Coastal salt marsh	Sandy beach	Sand dunes	Savanna	Treeless plains	Water	Wet rainforest	Total		
Dry rainforest	909	1	6	0	0	0	0	0	0	25	941	0.97	0.03
Grassland and sedgeland	0	605	39	2	0	12	13	10	0	6	687	0.88	0.12
Mangrove	46	50	642	0	0	1	1	0	0	8	748	0.86	0.14
Coastal salt marsh	0	6	1	292	11	0	0	0	0	0	310	0.94	0.06
Sandy beach	0	0	0	5	395	20	0	0	0	0	420	0.94	0.06
Sand dunes	0	0	0	1	21	443	0	0	0	0	465	0.95	0.05
Savanna	4	22	5	0	0	5	905	8	0	8	957	0.95	0.05
Treeless plains	0	19	0	0	0	50	85	196	0	0	350	0.56	0.44
Water	0	0	0	0	1	0	0	0	414	0	415	1	0
Wet rainforest	183	1	5	0	0	0	19	0	0	386	594	0.65	0.35
Total	1142	704	698	300	428	531	1023	214	414	433	5887		
PA	0.8	0.86	0.92	0.97	0.92	0.83	0.88	0.92	1	0.89			
OE	0.2	0.14	0.08	0.03	0.08	0.17	0.12	0.08	0	0.11			

Model formulation

**Classification scheme:** Ecosystem Functional Group (level 3 of the Global Ecosystem typology)

**Satellite/sensor:** Landsat-9/OLI-2

**Covariate set:** Satellite image and additional covariates

PA: Producer's accuracy

UA: User's accuracy

OE: Omission error

CE: Commission error

894

895 Table S6.10. Confusion matrix for the ecosystem functional group classification model using  
 896 Sentinel-2 satellite imagery from the MSI sensor as the only covariates.

	Training points											UA	CE
	Dry rainforest	Grassland and sedgeland	Mangrove	Coastal salt marsh	Sandy beach	Sand dunes	Savanna	Treeless plains	Water	Wet rainforest	Total		
Dry rainforest	727	2	17	0	0	2	0	0	0	90	838	0.87	0.13
Grassland and sedgeland	0	419	14	3	0	5	18	8	0	2	469	0.89	0.11
Mangrove	55	60	522	0	0	1	0	0	0	69	707	0.74	0.26
Coastal salt marsh	0	3	1	285	5	1	0	0	2	0	297	0.96	0.04
Sandy beach	0	0	0	7	356	77	0	0	0	0	440	0.81	0.19
Sand dunes	0	0	0	2	61	286	0	7	0	0	356	0.80	0.20
Savanna	2	50	15	0	0	13	754	29	0	20	883	0.85	0.15
Treeless plains	0	111	3	0	2	145	220	170	0	1	652	0.26	0.74
Water	0	1	0	3	4	0	0	0	412	0	420	0.98	0.02
Wet rainforest	358	58	126	0	0	1	31	0	0	251	825	0.30	0.70
Total	1142	704	698	300	428	531	1023	214	414	433	5887		
PA	0.64	0.60	0.75	0.95	0.83	0.54	0.74	0.79	1.00	0.58			
OE	0.36	0.40	0.25	0.05	0.17	0.46	0.26	0.21	0.00	0.42			

Model formulation

**Classification scheme:** Ecosystem Functional Group (level 3 of the Global Ecosystem typology)

**Satellite/sensor:** Sentinel-2/MSI

**Covariate set:** Satellite image covariates only

PA: Producer's accuracy

UA: User's accuracy

OE: Omission error

CE: Commission error

897

898 Table S6.11. Confusion matrix for the ecosystem functional group classification model using  
 899 Sentinel-2 satellite imagery from the MSI sensor and using satellite image and additional  
 900 covariates.

	Training points										Total	UA	CE
	Dry rainforest	Grassland and sedgeland	Mangrove	Coastal salt marsh	Sandy beach	Sand dunes	Savanna	Treeless plains	Water	Wet rainforest			
Dry rainforest	951	1	11	0	0	1	2	0	0	31	997	0.95	0.05
Grassland and sedgeland	1	532	28	3	0	20	18	9	0	2	613	0.87	0.13
Mangrove	57	106	648	0	0	3	1	0	0	7	822	0.79	0.21
Coastal salt marsh	0	6	1	291	6	4	0	0	0	0	308	0.94	0.06
Sandy beach	0	0	0	5	391	34	0	0	0	0	430	0.91	0.09
Sand dunes	0	0	0	1	30	402	2	3	0	0	438	0.92	0.08
Savanna	1	37	5	0	0	7	900	9	0	21	980	0.92	0.08
Treeless plains	0	20	0	0	0	60	86	193	0	0	359	0.54	0.46
Water	0	0	0	0	1	0	0	0	414	0	415	1.00	0.00
Wet rainforest	132	2	5	0	0	0	14	0	0	372	525	0.71	0.29
Total	1142	704	698	300	428	531	1023	214	414	433	5887		
PA	0.83	0.76	0.93	0.97	0.91	0.76	0.88	0.90	1.00	0.86			
OE	0.17	0.24	0.07	0.03	0.09	0.24	0.12	0.10	0.00	0.14			

Model formulation

**Classification scheme:** Ecosystem Functional Group (level 3 of the Global Ecosystem typology)

**Satellite/sensor:** Sentinel-2/MSI

**Covariate set:** Satellite image and additional covariates

PA: Producer's accuracy

UA: User's accuracy

OE: Omission error

CE: Commission error

901

902 Table S6.12. Confusion matrix for the biome classification model using Landsat-9 satellite  
 903 imagery from the OLI-2 sensor as the only covariates.

		Training points									UA	CE
		Grassland and sedgeland	Mangrove	Rainforest	Sandy beach	Sand dune	Savanna	Treeless plains	Water	Total		
Predicted type	Grassland and sedgeland	554	48	16	0	3	22	5	0	648	0.85	0.15
	Mangrove	38	867	130	9	0	3	0	2	1049	0.83	0.17
	Rainforest	10	60	1407	0	0	15	0	0	1492	0.94	0.06
	Sandy beach	0	11	0	375	100	0	0	0	486	0.77	0.23
	Sand dunes	1	2	0	42	319	0	4	0	368	0.87	0.13
	Savanna	49	10	22	0	15	848	39	0	983	0.86	0.14
	Treeless plains	51	0	0	0	94	135	166	0	446	0.37	0.63
	Water	1	0	0	2	0	0	0	412	415	0.99	0.01
	Total	704	998	1575	428	531	1023	214	414	5887		
	PA	0.79	0.87	0.89	0.88	0.60	0.83	0.78	1.00			
OE	0.21	0.13	0.11	0.12	0.40	0.17	0.22	0.00				

Model formulation

**Classification scheme:** Biome (level 2 of the Global Ecosystem typology)

**Satellite/sensor:** Landsat-9/OLI-2

**Covariate set:** Satellite image covariates only

PA: Producer's accuracy

UA: User's accuracy

OE: Omission error

CE: Commission error

904

905 Table S6.13. Confusion matrix for the biome classification model using Landsat-9 satellite  
 906 imagery from the OLI-2 sensor and using satellite image and additional covariates.

		Training points									UA	CE
		Grassland and sedgeland	Mangrove	Rainforest	Sandy beach	Sand dune	Savanna	Treeless plains	Water	Total		
Predicted type	Grassland and sedgeland	616	60	17	0	15	14	8	0	730	0.84	0.16
	Mangrove	43	907	31	6	9	1	0	0	997	0.91	0.09
	Rainforest	1	16	1443	0	2	13	0	0	1475	0.98	0.02
	Sandy beach	0	8	0	402	20	0	0	0	430	0.93	0.07
	Sand dunes	0	2	1	19	429	0	0	0	451	0.95	0.05
	Savanna	21	5	83	0	5	911	8	0	1033	0.88	0.12
	Treeless plains	23	0	0	0	51	84	198	0	356	0.56	0.44
	Water	0	0	0	1	0	0	0	414	415	1.00	0.00
	Total	704	998	1575	428	531	1023	214	414	5887		
	PA	0.88	0.91	0.92	0.94	0.81	0.89	0.93	1.00			
	OE	0.12	0.09	0.08	0.06	0.19	0.11	0.07	0.00			

Model formulation

**Classification scheme:** Biome (level 2 of the Global Ecosystem typology)

**Satellite/sensor:** Landsat-9/OLI-2

**Covariate set:** Satellite image and additional covariates

PA: Producer's accuracy

UA: User's accuracy

OE: Omission error

CE: Commission error

907

908 Table S6.14. Confusion matrix for the biome classification model using Sentinel-2 satellite  
 909 imagery from the MSI sensor as the only covariates.

		Training points									UA		CE	
		Grassland and sedgeland	Mangrove	Rainforest	Sandy beach	Sand dune	Savanna	Treeless plains	Water	Total				
Predicted type	Grassland and sedgeland	449	58	24	0	6	20	9	0	566	0.79	0.21		
	Mangrove	64	809	143	4	2	0	0	0	1022	0.79	0.21		
	Rainforest	23	92	1358	0	3	5	0	0	1481	0.92	0.08		
	Sandy beach	0	8	0	357	74	0	0	4	443	0.81	0.19		
	Sand dunes	0	2	0	60	290	0	6	0	358	0.81	0.19		
	Savanna	59	22	50	0	14	786	30	0	961	0.82	0.18		
	Treeless plains	107	4	0	3	142	212	169	0	637	0.27	0.73		
	Water	2	3	0	4	0	0	0	410	419	0.98	0.02		
	Total	704	998	1575	428	531	1023	214	414	5887				
	PA	0.64	0.81	0.86	0.83	0.55	0.77	0.79	0.99					
	OE	0.36	0.19	0.14	0.17	0.45	0.23	0.21	0.01					

Model formulation

**Classification scheme:** Biome (level 2 of the Global Ecosystem typology)

**Satellite/sensor:** Sentinel-2/MSI

**Covariate set:** Satellite image covariates only

PA: Producer's accuracy

UA: User's accuracy

OE: Omission error

CE: Commission error

910

911 Table S6.15. Confusion matrix for the biome classification model using Sentinel-2 satellite  
 912 imagery from the MSI sensor and using satellite image and additional covariates.

		Training points									UA	CE
		Grassland and sedgeland	Mangrove	Rainforest	Sandy beach	Sand dune	Savanna	Treeless plains	Water	Total		
Predicted type	Grassland and sedgeland	580	80	20	1	32	14	9	0	736	0.79	0.21
	Mangrove	65	880	33	4	19	0	0	0	1001	0.88	0.12
	Rainforest	0	27	1482	0	1	8	0	0	1518	0.98	0.02
	Sandy beach	0	7	0	396	33	0	0	0	436	0.91	0.09
	Sand dunes	1	1	0	26	378	1	1	0	408	0.93	0.07
	Savanna	36	3	40	0	6	911	8	0	1004	0.91	0.09
	Treeless plains	22	0	0	0	62	89	196	0	369	0.53	0.47
	Water	0	0	0	1	0	0	0	414	415	1.00	0.00
	Total	704	998	1575	428	531	1023	214	414	5887		
	PA	0.82	0.88	0.94	0.93	0.71	0.89	0.92	1.00			
OE	0.18	0.12	0.06	0.07	0.29	0.11	0.08	0.00				

Model formulation

**Classification scheme:** Biome (level 2 of the Global Ecosystem typology)

**Satellite/sensor:** Sentinel-2/MSI

**Covariate set:** Satellite image and additional covariates

PA: Producer's accuracy

UA: User's accuracy

OE: Omission error

CE: Commission error

## 913 Additional references

914 Aybar, C., Wu, Q., Bautista, L., Yali, R. and Barja, A. (2020) 'rgee: An R package for interacting with Google Earth Engine', *Journal of Open Source*  
 915 *Software*, 5(51), p. 2272. Available at: <https://doi.org/10.21105/joss.02272>.

916 van den Brand, T. (2024) 'ggh4x: Hacks for "ggplot2"'. Available at: <https://CRAN.R-project.org/package=ggh4x>.

917 Campitelli, E. (2023) 'ggnewscale: Multiple Fill and Colour Scales in "ggplot2"'. Available at: <https://CRAN.R-project.org/package=ggnewscale>.

918 Dunnington, D. (2023) 'ggspatial: Spatial Data Framework for ggplot2'. Available at: <https://CRAN.R-project.org/package=ggspatial>.

919 Gorelick, N., Hancher, M., Dixon, M., Ilyushchenko, S., Thau, D. and Moore, R. (2017) 'Google Earth Engine: Planetary-scale geospatial analysis  
 920 for everyone', *Remote Sensing of Environment*, 202, pp. 18–27. Available at: <https://doi.org/10.1016/j.rse.2017.06.031>.

921 Greenwell, B.M. and Boehmke, B.C. (2020) 'Variable Importance Plots—An Introduction to the vip Package', *The R Journal*, 12(1), pp. 343–366.  
 922 Available at: <https://doi.org/10.32614/RJ-2020-013>.

923 Henry, L., Wickham, H. and Chang, W. (2024) 'ggstance: Horizontal "ggplot2" Components'. Available at: <https://CRAN.R-project.org/package=ggstance>.

925 Hernangomez, D. (2024) 'tidyterra: tidyverse Methods and ggplot2 Helpers for terra Objects'. Available at:  
 926 <https://dieghernan.github.io/tidyterra/>.

927 Hijmans, R.J. (2023) 'terra: Spatial Data Analysis'. Available at: <https://CRAN.R-project.org/package=terra>.

- 928 Kuhn, M. (2008) 'Building Predictive Models in R Using the caret Package', *Journal of Statistical Software*, 28(5), pp. 1–26. Available at:  
929 <https://doi.org/10.18637/jss.v028.i05>.
- 930 Pebesma, E. (2018) 'Simple Features for R: Standardized Support for Spatial Vector Data', *The R Journal*, 10(1), pp. 439–446. Available at:  
931 <https://doi.org/10.32614/RJ-2018-009>.
- 932 R Core Team (2018) 'R: A language and environment for statistical computing'. Vienna, Austria: R Foundation for Statistical Computing.
- 933 RStudio Team (2020) 'RStudio: Integrated Development for R'. Boston, MA: RStudio, PBC. Available at: <http://www.rstudio.com>.
- 934 Smith, A., Murphy, S., Herderson, D. and Erickson, K. (2023) 'Including imprecisely georeferenced specimens improves accuracy of species  
935 distribution models and estimates of niche breadth', *Global Ecology & Biogeography*, 32(3), pp. 342–355. Available at:  
936 <https://doi.org/doi:10.1111/geb.13628>.
- 937 Wickham, H. (2016) 'ggplot2: Elegant Graphics for Data Analysis.' New York: Springer-Verlag.
- 938 Wickham, H. (2022) 'stringr: Simple, Consistent Wrappers for Common String Operations'. Available at: [https://CRAN.R-](https://CRAN.R-project.org/package=stringr)  
939 [project.org/package=stringr](https://CRAN.R-project.org/package=stringr).
- 940 Wickham, H., François, R., Harry, L., Müller, K. and Vaughan, D. (2023) 'dplyr: A Grammar of Data Manipulation'. Available at: [https://CRAN.R-](https://CRAN.R-project.org/package=dplyr)  
941 [project.org/package=dplyr](https://CRAN.R-project.org/package=dplyr).
- 942 Wickham, H., Vaughan, D. and Girlich, M. (2023) 'Tidyr: tidy messy data'. Available at: <https://CRAN.R-project.org/package=tidyr>.
- 943 Wright, M.N. and Ziegler, A. (2017) 'Ranger: a fast implementation of random forests for high dimensional data in C++ and R.', *Journal of*  
944 *Statistical Software*, 77(1), pp. 1–17. Available at: <https://doi.org/doi:10.18637/jss.v077.i01>.
- 945